國立交通大學

分子醫學與生物工程研究所

碩士論文

克雷白氏肺炎桿菌 CG43 中尿嘧啶雙磷酸葡萄糖去氫酶之酪胺酸磷酸化的角色

Role of tyrosine phosphorylation on the UDP-glucose dehydrogenase of *Klebsiella pneumoniae* CG43

研究生：葉家華　(Jia-Hua Yeh)

學號：9729503

指導教授：彭慧玲　博士　(Hwei-Ling Peng)

中華民國九十九年六月

中文摘要

克雷白氏肺炎桿菌為一伺機性感染的格蘭氏陰性菌，可藉其外部包覆的厚重多醣體莢膜躲避細胞的吞噬作用及避免被血清因子所毒殺。我們先前的研究證實克雷白氏肺炎桿菌蛋白質酪胺酸激酶(Wzc)可藉由磷酸化尿嘧啶雙磷酸葡萄糖去氫酶(UDP-glucose dehydrogenase, Ugd)來提升 Ugd 酵素活性，進而調控莢膜多醣體的生成；而在 Ugd 上的 17 個酪胺酸殘基，已被選取作定點突變的 9 個酪胺酸殘基的改變並未影響 Ugd 的磷酸化。為了確認 Ugd 上被磷酸化的酪胺酸殘基，本研究將其他 8 個酪胺酸殘基，分別在 53、71、76、85、203、252、302 和 380 的位置，經點突變技術換成苯丙胺酸。再將這幾個定點突變後的蛋白質表現純化後，利用西方墨點法發現這些突變株仍能在大腸桿菌體內被磷酸化，此結果顯示克雷白氏肺炎桿菌不同於已報導的大腸桿菌與枯草桿菌，可能具有不只一個可受磷酸化的酪胺酸殘基。同時，酵素活性與動力學特性的分析結果得知，Tyr71、Tyr85、Tyr252 和 Tyr380 的突變明顯影響了 Ugd 酵素活性，而這些點突變蛋白經由(circular dichroism, CD)圖譜分析，確認其二級結構組成與野生型 Ugd 無顯著差異，暗示著這些酪胺酸殘基的改變可能因無法被磷酸化而降低 Ugd 活性。

Abstract

Klebsiella pneumoniae, an opportunistic gram-negative bacterial phathogen, is mostly encapsulated by a thick capsular polysaccharide (CPS) which acting to protect the bacterium from phagocytosis and prevent from damage by serum factors. Via an *in vitro* phosphorylation assay, we have previously demonstrated the protein-tyrosine kinase, Wzc, was capable of phosphorylating the enzyme UDP-glucose dehydrogenase (Ugd) to increase the enzymatic activity. The Ugd phosphorylation led to increase of the synthesis of CPS. Nine of the 17 tyrosine residues on *Kp*Ugd have been substituted individually with phenylalanine by site-directed mutagenesis. However, *in vitro* phosphorylation assay revealed that none of the changes affected the Ugd phosphorylation. Here, we generate specific mutation on the rest of the tyrosine residues on Ugd. Interestingly, all of the mutant proteins, Y53F, Y71F, Y76F, Y85F, Y203F, Y252F, Y302F, and Y380F, isolated from *E. coli* appeared to be phosphorylated. This suggested that *Kp*Ugd carried an additional tyrosine phosphorylation residue except the one reported for *Ec*Ugd-Y71 and *Bs*Ugd-Y70. Nevertheless, the enzyme kinetics analysis revealed that UgdY71F, UgdY85F, UgdY252F, and UgdY380F exhibit much lower activity than wild type Ugd. Circular dichroism analysis of the mutant Ugd indicated that the reduced activity was not due to structural alteration, implying the change of Y85, Y252, or Y380 impaired the subjection to phosphorylation leading to the decreased activity.

致謝

真的(*￣▽￣)/・★*"‘’*-.,)我完成我的碩士論文哩！致謝對我來說，是一篇論文完美的ending，同時也說明著一篇論文從開始到結束所面臨的難關，以及對協助渡過難關的恩人們感謝。回顧這兩年，歡樂與淚水還有在實驗室鬼吼鬼叫 └(｀。´＊)┘ 失控狀態的交織下，譜出了我永遠難忘的碩士生涯。

這篇論文得以順利完成，首先要感謝我的老闆－彭慧玲博士。老師在我碩一11月漂泊無助時，將我拎回實驗室進行培養，加入彭家這可愛的大家庭。很感謝老師總在我遇到困難時，帶領我一起”問問題”，找出癥結與解決的辦法，提供我實質和精神上的幫助。古人云：「一日為師，終身為母。」這句話用來形容我最不為過。老師～謝謝您的照顧與關懷！請好好照顧您的身體，不要讓我們擔心哩！

再來，誠心感謝實驗室的成員。首先是平易近人的丸子太后：很享受和你一起在早晨霸占實驗室的時光，把你餵飽飽看你開心我也跟著快樂ㄟ(￣▽￣ㄟ)。謝謝在實驗上你對我得教導，希望一同離開實驗室的你可以找到幸福與喜歡的工作；謝謝建誠與小新學長對我實驗上的幫忙與平日的照顧，並將實驗室運作得井然有序；謝謝美麗且腿超級長的靜柔學姊，在我初進實驗室時，帶領我做實驗與熟悉環境，沒有妳我沒辦法那麼快融入這家庭；謝謝雅雯跟顗峰像母雞帶小雞般

的關心、照顧；謝謝寡言的其駿，大家齊聚你家烤肉的歡樂畫面如昨日歷歷；謝謝可愛的品宣與酷酷的葳云，實驗室的活力就靠你們繼續維持；謝謝老派的豪君，希望你能將我們磷酸化研究系列發揚光大；超級特別感謝佩君與哲充，你們兩是我碩士生涯的一大部分，沒有你們一定會黯淡無聊許多。我不會忘記哲充師傅使出渾身解數教我實驗技巧，希望你能夠在心靈上不斷成熟，有朝一日變成能獨當一面的實驗室一哥。謝謝我的好麻吉佩君((>(´‿ `*)<)))，很榮幸能夠認識那麼充滿歡笑氣質的你，一起實驗一起瘋狂、一起歡樂一起難過一起畢業，希望哪天你能駕著黑頭車載我一起去吃貴婦下午茶。謝謝分子調控實驗室歷來所有的成員，有你們才有我順遂的碩士生涯。

謝謝張晃猷老師與其實驗室成員在我研究上給予的建議與幫助。

謝謝楊裕雄老師能夠騰出時間擔任口試委員，指導論文的修正。

謝謝貼心的恒毅v(￣‿￣)y陪在我身邊守護、鼓勵、照顧我！

最後，感謝我的家人給我的支持與關愛，我把碩士這份榮耀獻給你們，我不會讓你們失望的。

當學生的日子終告一個段落，o(〒﹏〒)o能夠遇見大家真是太幸運哩！希望哪天相聚時，大家依舊過的很幸福很快樂！

家華　謹致於

交通大學分子醫學與生物工程研究所　中華民國九十九年六月

Contents

Table contents

Figure contents

Abbreviation

ATP	adenosine triphosphate
BCIP	5- bromo-4-chloro-3-indolyl phosphate
bp	base pair
CFU	colony forming unit(s)
CIAP	calf intestine alkaline phosphatase
CPS	capsular polysaccharide
DNA	deoxyribonucleic acid
DTT	dithiothreitol
EDTA	ethylenediamine-tetraacetic acid
EPS	exopolysaccharide
IPTG	isopropyl-1-thio-β-D-galactopyranoside
kb	kilobase(s)
kDa	kiloDalton(s)
LB	Luria-Bertani
μM	micromolar
mM	millimolar
NAD^+	nicotinamide adenine dinucleotide
NADH	nicotinamide adenine dinucleotide (reduced form)
NBT	nitro blue tetrazolium chloride
ORF	open reading frame
PAGE	polyacrylamide gel electrophoresis
PBS	phosphate buffered saline
PCR	polymerase chain reaction
PTK	protein-tyrosine kinase

PTP	protein-tyrosine phosphatase
PVDF	polyvinylidene difluoride
rpm	revolutions per minute
SDS	sodium dodecyl sulfate
UDP	uridine 5'-diphosphate
UDP-Glc	UDP-glucose
UDP-GlcUA	UDP-glucuronic acid
Ugd	UDP-glucose dehydrogenase

Introduction

Klebsiella pneumoniae

Klebsiella pneumoniae, a member of the *Enterobacteriaceae* family, is a non-motile, facultative anaerobic, and rod-shape bacterium. Their environmental habitats are surface water, sewage, soil and on plants (Brown and Seidler 1973; Seidler, Knittel *et al*., 1975). *K. pneumoniae* is responsible for a variety of diseases in humans and animals (Brisse *et al*., 2006). Most notoriously, it is a prominent nosocomial pathogen (causing community-acquired diseases including bacteremia, septicemia, urinary, respiratory and blood infections) and the agent of specific human infections including Friedla¨nder's pneumonia, rhinoscleroma and the emerging disease pyogenic liver abscess (PLA), occurring particularly in immunocompromised patients (Podschun and Ullmann, 1998; Brisse *et al*., 2009). Other *K. pneumoniae* infections that are severe but more rarely reported include meningitis, necrotizing fasciitis and prostatic abscess (Lu *et al*., 2002; Kohler *et al*., 2007). Finally, granuloma inguinale (donovanosis) (Richens, 1985) is caused by uncultivated bacteria, which may belong to *K. pneumoniae* (Grimont, 2005).

Factors that are implicated in the virulence of *K. pneumoniae* strains include the capsular serotype, lipopolysaccharide, iron-scavenging systems, and fimbrial and non-fimbrial adhesins (Regue *et al*., 2001; Chou *et al*., 2004; Ma *et al*., 2005). Most *Klebsiella* strains are encapsulated by a polysaccharidic capsule of considerable thickness responsible for the glistening and mucoid colonies on agar plates. The abundant polysaccharidic capsule protects against the bactericidal action

of serum and impairs phagocytosis, and may be regarded as the most important virulence determinant of *K. pneumoniae*.

K. pneumoniae could be classified into 77 serological K antigen types according to the diverse structure of the capsular polysaccharides (Ørskov and Ørskov, 1984). The K1/K2 strains were found to be especially pathogenic in causing PLA, a common intra-abdominal infection with 10-30% high mortality rate worldwide (Fung *et al*., 2002). Other serotypes showed little or no effect in PLA pathogenesis (Mizuta *et al*., 1983). The highly virulent clinical isolates are often carry large capsules as an important virulence factor to protect the bacteria from opsonophagocytosis and prevent from complement-mediated killing (Simoons-Smit *et al*., 1986).

Capsular polysaccharides and *cps* genes regulation

K. pneumoniae CG43, showing a strong virulence to Balb/c mice with 50% lethal dose of 10 CFU, is a highly encapsulated clinical isolate of K2 serotype (Chang *et al.*, 1996). The structure of the K2 capsular polysaccharides (CPS) has been determined as $[\rightarrow)4\text{-Glc-}(1\rightarrow3)\text{-}\alpha\text{-Glc-}(1\rightarrow4)\text{-}\beta\text{-Man-}(3\leftarrow1)\text{-}\alpha\text{-GlcA)-}(1\rightarrow]_n$ (Wacharotayankun *et al.*, 1992), which is made from a similar biosynthetic pathway to that of *Escherichia coli* group 1 CPS (Whitfield and Roberts, 1999). In *E. coli*, four groups of CPS biosynthesis pathways could be identified. Group 1 and 4 CPS synthesis requires a Wzx/Wzy dependent pathway: the repeat unit oligosaccharide is transferred to a lipid carrier, undecaprenyl phosphate (und-P), forming und-PP-linked

repeat units, which flips across the inner membrane in a process requiring Wzx. The polymer is formed in Wzy-dependent polymerization, as the growing chain is transferred to und-PP-linked unit. Then, polymer is translocated by Wza, the outer membrane protein. The biosynthesis of group 2 and 3 CPS is ATP-binding-cassette (ABC) transporter-dependent, of which the diacylglycerophosphate-linked repeat unit is produced by glycosyltransferase followed by the export of polymer across inner membrane via ABC transporter (Whitfield, 2006).

The K2 *cps* (capsular polysaccharide synthesis) gene cluster of *K. pneumoniae* Chedid has been determined, which contains 19 open reading frames (ORFs) organized into 3 transcriptional units (Arakawa *et al.*, 1995). Among these genes, *orf3* to *orf6*, a highly conserved gene-block, are counterparts of *E. coli wzi-wza-wzb-wzc* (Rahn *et al.*, 1999). Wzi is an outer membrane protein and *wzi* mutant showed a significant reduction in cell-bound CPS polymer with a corresponding increase in cell-free material. This proposed that Wzi plays in the process that links high-molecular-weight capsule to the cell surface (Alvarez *et al.*, 2000; Rahn *et al.*, 2003). Wza is a periplasmic protein involved in forming a multimeric putative translocation channel. The *Orf5*, *Kp*Wzb, is a low molecular weight protein tyrosine phosphatase (PTP) and *Orf6*, *Kp*Wzc, a protein tyrosine kinase (PTK) that participated in high-level polymerization of capsular polysaccharide. Enzymatic activities of the two proteins, *Kp*Wzb and *Kp*Wzc, have already been demonstrated (Preneta *et al.*, 2002).

Protein phosphorylation on tyrosine in bacteria

Protein phosphorylation is one of the most important post-translational covalent modifications and has gained recognition as a key device in the pleiotropic regulation of multiple cellular functions in eukaryotic organisms (Hunter, 2000; Pawson and Scott, 2005). It is best known that protein phosphorylation is a reversible enzyme-catalyzed process which controlled by various kinases and phosphatases. The first two protein-phosphorylating systems, ‘‘two-component systems (2CS)’’ and ‘‘phosphotransferase system (PTS)’’ have been recognized as the hallmark of bacterial signaling (Deutscher et al. 2006; Klumpp and Krieglstein, 2002). The third phosphorylating system in bacteria closely resembles the ‘‘classical’’ ATP/GTP-dependent system in eukaryotes (Cozzone, 1998; Shi *et al*., 1998). In this system, proteins are phosphorylated on serine and/or threonine or tyrosine. Recently, accumulating evidences suggest that Ser/Thr/Tyr phosphorylations also contribute to the regulation of a diverse range of cellular responses and physiological processes in prokaryotes (Cozzone, 2005). Modification at serine/threonine is usually more frequent than modification at tyrosine (3-15%), but both types of modification appear to coexist in nearly all bacterial species (Sun *et al*., 2010).

Tyrosine phosphorylation is a key device in numerous cellular functions in eukaryotes, but in bacteria this protein modification was largely ignored until mid-1990s (Grangeasse *et al*., 2007). Recent data have shown that a variety of cellular processes essential for bacterial survival and virulence are regulated by the phosphorylation of certain

endogenous proteins (Cozzone, 2009). This reaction is catalyzed by autophosphorylating ATP-dependent protein-tyrosine kinases which use homologues of Walker motifs of nucleotide-binding proteins for their catalytic mechanism (Grangeasse *et al*., 2007). These kinases exhibit similar but not identical structural and functional features with their eukaryotic counterparts (Olivares-Illana *et al*., 2008; Lee *et al*., 2008). For antibacterial therapy, this is important because it opens the way to molecular characterization of specific ligands that would selectively block the enzymatic activity of bacterial kinases (Cozzone, 2009). Based on these features, most of them have been recently unified in a new enzyme family called Bacterial tyrosine kinase (BY-kinase), a typical BY-kinase containing a catalytic domain, Walker A and B motifs, and C-terminal tyrosine cluster. (Grangeasse *et al*., 2007).

Although BY-kinases from Gram-negative and Gram-positive bacteria exhibit significant sequence similarity, they possess different domain organizations. BY-kinases of Gram-negative bacteria are usually large proteins (~80 kDa) composed of an N-terminal transmembrane domain and a C-terminal cytosolic PTK domain containing the active site Walker motifs A and B (Doublet *et al.*, 1999, 2002). When expressed separately, the soluble C-terminal domain of *E. coli* Wzc still exhibits autophosphorylation activity (Grangeasse *et al.*, 2002). By contrast, PTKs of Gram-positive bacteria are naturally separated into two distinct proteins, *i.e.* a transmembrane protein with limited similarity to the N-terminal domain and a soluble protein with significant similarity to the C-terminal domain of PTKs from Gram-negative bacteria. The soluble

protein containing the Walker motifs A and B also autophosphorylates at a tyrosine cluster located in its C terminus (Macek *et al*., 2003). The different domain organization of PTKs between Gram-negative and Gram-positive bacteria has suggested a different regulation of these enzymes.

In terms of genomic organization, the genes encoding a protein-tyrosine kinase and a protein-tyrosine phosphatase in bacteria are most often located next to each other on the chromosome. In addition, these genes are generally part of large operons that direct the coordinate synthesis of proteins involved in the production or regulation of exopolysaccharides and capsular polysaccharides. Recent data provide evidence that there exists a direct relationship between the reversible phosphorylation of proteins on tyrosine and the production of these polysaccharidic polymers, which are involved in the early steps of the infection process and are considered potent virulence factors (Cozzone *et al*., 2004).

In the past, functional roles of the critical components involved in protein phosphorylation used to be defined by biochemical and genetic approaches (Cozzone, 2005). A salient gap exists between the growing number of identified protein-tyrosine kinases/phosphatases and the relative paucity of the protein substrates characterized to date (Lin *et al*., 2009). Nevertheless, in the past few years, high-performance techniques (based on gel-free peptide analysis and mass spectrometry) have been developed in association with systematic determination of genomic sequences for a fast identification of hundreds of phosphoproteins and

corresponding phosphorylation sites. They have been applied so far to the phosphoproteomes (*i.e.* the entire complement of phosphorylated proteins expressed by a cell) of *B. subtilis* (Macek *et al*., 2007), *E. coli* (Macek *et al*., 2008), *Lactococcus lactis* (Soufi *et al*., 2008), *Pseudomonas sp.* (Ravichandran *et al*., 2009) and *Klebsiella pneumoniae* (Lin *et al*., 2009).

These endogenous protein substrates are present in a wide array of metabolic and regulatory processes from genetic competence and gene transcription to morphogenesis and stress. They also participate in cell division and differentiation, motility, biofilm formation, sporulation, central metabolism, protein biosynthesis and antibiotic resistance (Cozzone, 2009). This discovery contributes to the emerging picture that bacterial tyrosine phosphorylation, in addition to the classical serine/threonine kinases, and the 2CS and PTS, is an important regulatory arsenal of bacterial physiology beyond its sole implication in pathogenesis.

The first known kinase substrates are the kinases themselves because they are autophosphorylating enzymes. The later identified protein is UDP-glucose dehydrogenases (Ugd) (Grangeasse *et al*.,2003; Mijakovic *et al*., 2003). Phosphorylation of the enzyme significantly increases the dehydrogenase activity thereby stimulates formation of the precursors for polysaccharide production, lipopolysaccharide modification for the resistance to cationic peptides or polymyxin-type antibiotics or phosphate metabolism in *E.coli* and *B. subtilis* (Breazeale *et al*., 2002; Soldo *et al*., 1999).

UDP-glucose dehydrogenase (Ugd)

UDP-glucose dehydrogenase (Ugd) catalyzes a two-step NAD^+-dependent oxidation of UDP-glucose to produce UDP-glucuronic acid (UDP-GlcUA). The mechanism of Ugd proceeds through an initial oxidation of UDP-glucose with transfer of the C6" *pro-R* hydride (H_R in Appendix 1) to the *si* face (B face) of NAD^+ to form NADH and the aldehyde intermediate (Feingold and Franzen, 1981). Covalent catalysis proceeds with nucleophilic attack of Cys 260 on the aldehyde to give a thiohemiacetal that is oxidized to a thioester intermediate by transfer of the remaining hydride (H_S in Appendix 1) to a second molecule of NAD^+. In the final step of the normal enzymatic reaction, the thioester intermediate is irreversibly hydrolyzed to give UDP-GlcUA. The importance of UDP-GlcUA is apparent considering the downstream polymers that utilize this compound or its derivates, such as UDP-xylose, UDP-arabinose, and UDP-galacturonic acid in a variety of organisms ranging from mammals to bacteria (Seifert, 2004).

In mammals, UDP-GlcUA is the substrate for UDP-glucuronosyl transferases in the liver that catalyze the formation of glucuronide conjugates with various substances such as bilirubin and thereby aid in their excretion (Dutton, 1980). UDP-GlcUA is also essential for the biosynthesis of hyaluronan and various glycosaminoglycans such as chondroitin sulfate and heparan sulfate (Roden, 1980). Mutation of the Ugd gene of *Drosophilia melanogaster* (designated sugarless) disrupts biosynthesis of the heparan sulfate side chains on proteoglycan core proteins and is identical in phenotype to the classical wingless mutation

(Binari *et al*., 1997). In plants, Ugd may be an important regulatory enzyme in the carbon flux toward cell wall and glycoprotein biosynthesis due to feedback inhibition from UDP-xylose (Dalessandro and Northcote, 1977).

In many pathogenic bacteria, UDP-GlcUA is a precursor and an essential component for the biosynthesis of exo- polysaccharides (EPS) and lipopolysaccharides (LPS). EPS or LPS is critical virulence factor which enables the bacteria to evade attacks by host immune system, such as phagocytosis (Cross, 1990; Moxon and Kroll, 1990; Watson and Musher, 1990; Wessels *et al*., 1994). UDP-GlcUA also participates in the production of UDP-4-amino-4-deoxy-Larabinose (L-Ara4N) which is a crucial element in bacterial resistance to antibiotics such as polymyxin and cationic peptides of the innate immune system (Breazeale *et al*., 2003).

Recent studies demonstrate that transcription of the *Salmonella* ugd is controlled by three regulatory systems that respond to different signals (Mouslim *et al*., 2003). Ugd mutation in the pathogenic fungus *Cryptococcus neoformans* alters the cell integrity and nucleotide sugar pool. The cells also become temperature-sensitive and fail to grow in an animal model (Griffith *et al*., 2004). *Pseudomonas aeruginosa* PAO1 encodes two Ugd, *PA2022* and *PA3559*. The *PA2022* mutant and *PA2022-PA3559* double mutant, but not the *PA3559* mutant, are more susceptible to chloramphenicol, cefotaxime, and ampicillin. The *PA3559* mutant, however, shows a reduced resistance to polymyxin B compared with wild type PAO1(Hung *et al*., 2007). In *E.coli*, phosphorylation of

Ugd by Wzc plays a role in the regulation of the amount of the EPS colanic acid, whereas Etk-mediated Ugd phosphorylation participates in the resistance to the polymyxin (Lacour *et al*., 2008).

Activity of other dehydrogenases, including *Bacillus subtilis* Ugd (Mijakovic *et al*., 2004) and the UDP acetyl-mannosamine dehydrogenase CapO of *Staphylococcus aureus* (Soulat *et al*., 2007), have recently been shown to be regulated by tyrosine-phosphorylation. It is hence speculated that tyrosine phosphorylation of this class of enzymes is a common regulatory mechanism found in bacteria.

Identification of the phosphotyrosine residues

Although a lot of protein kinases and phophatases have been predicted and identified in a variety of bacterial species, classical biochemical approaches have so far revealed only a few substrate proteins and even fewer phosphorylation sites. In previous work, we have provided *in vitro* evidence that the Wzc of *K. pneumoniae* CG43 (*Kp*Wzc) was able to phophorylate Ugd the phosphorylation appeared to enhance the Ugd activity (Appendix 2, Zhi-Kai Li, 2006). To advance our knowledge of the underlying mechanism in capsule formation for the development of new therapeutic strategies, it is crucial to identify the phosphorylation site on Ugd. The previously employed mass spectrometry analysis (MALDI-TOF) failed to identify the Ugd phosphorylated tyrosine probably because of the low occupancy of bacterial phosphorylation sites (Macek *et al*., 2006). Nevertheless, a most recently study of the *Bacillus subtilis* phosphoproteome indicated that

Ugd was phosphorylated *in vivo* on tyrosine 70 (Macek *et al*., 2007). Tyrosine 71, the counterpart residue of *Ec*Ugd was later demonstrated as the specific phosphorylation residue (Lacour *et al*., 2008). As shown in Fig. 1, multiple sequence alignment suggested the Tyrosine 71 (Tyr71) of *Kp*Ugd sequence is the phosphorylation site.

The sequence alignments of Ugd from *K. pneumoniae*, *E. coli* K-12, *S. pyogenes*, *B. subtilis*, *E. amylovora*, and *S. pneumoniae* revealed nine conserved tyrosine residues Tyr10, Tyr91,Tyr150, Tyr210, Tyr217, Tyr242, Tyr249, Tyr265 and Tyr335. We have previously tried to generate site-directed mutation, tyrosine changed to phenylalanine, on Ugd targeting to the 9 residues (Mei-Ju Li, 2008). However, the *in vitro* phosphorylation assays indicated that all the mutated proteins were able to be phosphorylated by the catalytic domain of Wzc, Wzc_{cyto}, although some of the mutations had slightly changed the Ugd activity,

Here, the rest of the eight tyrosine residues on *Kp*Ugd (Tyr53, Tyr71, Tyr76, Tyr85, Tyr203, Tyr252, Tyr302, and Tyr380) were subjected to site-directed mutagenesis. Phosphorylation assay was then employed to analyze the mutant proteins carrying with each of the alterations. In the mean time, the enzymatic activity determined if Tyr71 is the only phosphorylation site and if any of the tyrosine residues plays a role in influencing the Ugd activity.

Materials and methods

Bacterial Strains, Plasmids, and Growth Conditions

Genomic DNA prepared from *K. pneumoniae* CG43 was used as template for PCR amplification of the *ugd* gene. Bacterial strains and plasmid used in this study are listed in Table 1. *K. pneumoniae* CG43 is a clinical isolates recovered from Chang Gung Memorial Hospital, Linkou. All strains were routinely cultured at 37°C in Luria-Bertani (LB; 10 g/l tryptone, 5 g/l yeast extract, 10 g/l sodium chloride) broth or on LB agar. The following antibiotic concentrations were used: Kanamycin 25 μg/ml, Ampicillin 100 μg/ml, Tetracycline 20 μg/ml and Streptomycin 50 μg/ml. The plasmid generated and primers used are listed in Table 2 and Table 3, respectively.

Recombinant DNA manipulation

All recombinant DNA experiments were carried out by standard procedures as described (Sambrook *et al*., 2001). Restriction endonucleases and DNA modifying enzymes were purchased from MBI Fermentas (Hanover, MD) or New England Biolab (Beverly, MA, USA), and were used according to the recommendation by the suppliers. Plasmids were purified by using the High-Speed Plasmid Mini kit (Geneaid, Taiwan). PCR amplifications were performed with Taq DNA polymerase (MDBio, Inc, Taiwan). PCR products and DNA fragments were purified using the Gel/PCR DNA Fragments Extraction kit (Geneaid, Taiwan). The primers used in this study were synthesized by MDBio, Inc, Taiwan.

Construction for the overproduction of His_6-tagged Ugd and the derived mutants

The Ugd mutants were generated using QuikChange site-directed mutagenesis method (Stratagene). The procedure utilized the yT&A vector with an insert of *ugd* and two synthetic oligonucleotide primers containing the desired mutation. The oligonucleotide primers, each complementary to opposite strands of the vector, were extended during temperature cycling by Finnzymes' Phusion™ High-Fidelity DNA polymerase. Incorporation of the oligonucleotide primers generated a mutated plasmid containing staggered nicks. Following temperature cycling, the product is treated with *Dpn* I. The *Dpn* I endonuclease (target sequence: 5´-Gm6ATC-3´) is specific for methylated and hemimethylated DNA and is used to digest the parental DNA template and to select for mutation-containing synthesized DNA. The nicked vector DNA containing the desired mutations is then transformed into *E.coli* JM109 (Appendix 3).

The plasmid was then subcloned into the pET-30b expression vector at *Eco*R Ⅰ /*Sal* Ⅰ restriction sites to be in-frame with the His_6 tag at the N terminus of the protein. The constructs were then introduced into *E. coli* NovaBlue (DE3) by the heat shock method, and the transformants were selected on LB agar containing 25 μg/ml Kanamycin. The DNA was sequenced to verify the correctness of the cloned gene and the reading frame fusion with the His_6 tag. The resulting plasmids were named pET30UgdY53F, pET30UgdY71F, pET30UgdY76F, pET30UgdY85F,

pET30UgdY203F, pET30UgdY252F, pET30UgdY302F, pET30UgdY380F and the mutants Ugd proteins were expressed in *E.coli* NovaBlue (DE3).

Overproduction and purification of the His_6-Ugd and the derived mutants

The bacterial cells were incubated in 100 ml of LB medium supplemented with Kanamycin at 37°C with shaking until OD_{600} reached 0.5~0.6. Isopropyl-1-thio-β-D-galactopyranoside (IPTG) was then added to a final concentration of 1 mM and the growth was continued for 4 h at 37°C. Subsequently, the cells were harvested by centrifugation at 5000 rpm for 10 min, resuspended in binding buffer (20 mM Tris-HCl, 500 mM NaCl, 5 mM imidazole, pH 7.9), and the cell suspension disrupted by sonication and then the cell debris removed by centrifugation at 13000 rpm for 20 min. Finally, the His_6-tagged proteins were purified from the supernatant via affinity chromatography using His-Bind resin (Novagen), and the elution was carried out with elute buffer (20 mM Tris-HCl, 500 mM NaCl, 1 M imidazole, pH 7.9). Aliquots of the collected fractions were analyzed by SDS-PAGE and the fractions containing most of the purified His_6-tagged Ugd were dialyzed against the buffer containing 50 mM Tris-HCl (pH7.5), 100 mM NaCl, 1 mM EDTA, and 10% (v/v) glycerol.

Overproduction and purification of His_6 tag fusion *Kp*Wzc cytoplasmic domain

E.coli BL21-RIL cells were transformed with pET30-*Kp*WzcE23 (Table 2), which expressing a mutated *Kp*Wzc cytoplasmic domain, His_6-*Kp*Wzc (Arg^{451}-Lys^{722}). Overproduction for His_6-*Kp*Wzc was carried out with similar conditions for Ugd except IPTG was added to a final concentration of 0.5mM. Subsequently, the cells were harvested by centrifugation at 5000 rpm for 10 min, resuspended in binding buffer (50 mM sodium phosphate, 300 mM NaCl, 10 mM imidazole, 10% (v/v) glycerol, pH 8.0), and the cells disrupted by sonication and then the cell debris removed by centrifugation at 13000 rpm for 20 min. Finally, the His_6-*Kp*Wzc were purified from the supernatant via affinity chromatography using His-Bind resin (Novagen), and the elution was carried out with elute buffer (50 mM sodium phosphate, 300 mM NaCl, 100 mM imidazole, 10% glycerol, pH 8.0). Aliquots of the collected fractions were analyzed by SDS-PAGE and the fractions containing most of the purified His_6-*Kp*Wzc were dialyzed against the buffer containing 50 mM sodium phosphate (pH 8.0), 150 mM NaCl, 5 mM $MgCl_2$, 5 mM dithiothreitol and 10% (v/v) glycerol.

SDS-polyacrylamide gel electrophoresis

Protein preparation were treated for 10 min at 95°C in loading buffer (0.0626 M Tris-HCl buffer pH 6.8, 2% (v/v) SDS, 10% (v/v) glycerol, 0.01% (v/v) bromophenol blue, and 100 mM dithiothreitol). Twenty microliters of sample was applied to a 12.5% (v/v) SDS polyacrylamide

slab gel. Electrophoresis was carried out at room temperature until the tracking dye ran off the bottom of the slab gel. The gel was stained for 5 min using solution containing 2.5% (v/v) Coomassie Blue R250, 45% (v/v) methanol, and 10% (v/v) acetic acid, and destained in destain buffer (40% (v/v) methanol and 10% (v/v) acetic acid) for 30 mins.

In vitro phosphorylation assay

The phosphorylation assay was carried out essentially as described (Appendix 4, Grangeasse *et al*., 2003). Briefly, the 20 µl reaction mixtures contains about 2 µg of the purified wild-type Ugd or mutant Ugd, 2 µg kinase and 10 µM ATP in 25 mM Tris-HCl (pH 7.0), 1 mM DTT, 5 mM $MgCl_2$, 1 mM EDTA was incubated at 37 °C for 1h. The reaction was stopped by addition of the sample buffer and heated at 95°C for 5 min. After electrophoresis (12.5% SDS-PAGE), the gel was analyzed by western blotting or stained with Pro-Q® Diamond Phosphoprotein fluorescent dye (Invitrogen, catalog # P33300) for detection of the phosphorylated proteins and the result visualized using Amersham Typhoon™ 9200 Imager.

Western blot analysis of the phosphotyrosine proteins

The purified proteins were analyzed by SDS-PAGE and the resolved proteins were transferred to a polyvinylidene difluoride (PVDF) membrane electrophoretically in the transfer buffer containing 137 mM NaCl, 2.7 mM KCl, 10 mM Na_2HPO_4, 2 mM KH_2PO_4 and 20% methanol. The membrane was detected by the anti-phosphotyrosine clone 4G10

antibody (Upstate, catalog # 05-321) and the secondary antibody, an anti-mouse IgG alkaline phosphatase conjugated antibody (Sigma), was then applied and the bound complex was detected by using nitro blue tetrazolium chloride (NBT)/5-bromo-4-chloro-3-indolyl phosphate (BCIP) as the substrates.

Enzyme activity measurement and the kinetics characterization

UDP-glc dehydrogenase activity was determined by monitoring the change in absorbance at 340 nm that accompanies the reduction of NAD^+ to NADH using a spectrophotometric assay as described (Pagin *et al*., 1999). The enzyme assay was performed at room temperature in 100 mM Tris-HCl (pH 9.0), 100 mM NaCl, 2 mM DTT, 2 mM NAD^+ and 5 mM UDP-glc. The K_m and V_{max} for UDP-glc and NAD^+ were determined independently using standard assay conditions. Kinetic study for UDP-glc as the substrate was performed with a fixed concentration of NAD^+ and the concentration of UDP-glc varied in the range from 0.01 to 5 mM. Similarly, NAD^+ kinetic measurement was made by holding UDP-glc concentration and varying NAD^+ from 0.005 to 2 mM. K_m and V_{max} were calculated by fitting the data to the equation ($V = V_{max}[S]^h / ([S]^h + K_m{}^h)$), where h is the Hill coefficient, and assuming a single binding site each for substrate and cofactor.

Circular dichroism spectrum analysis

The interaction of a chiral molecule with polarized light is very specific and has proved to be an important method for characterizing both

small molecule and macromolecular structures (Fasman, 1996). Essentially, one type of measurements commonly made to determine the effects of polarized light on asymmetric molecules is circular dichroism (Hammes, 2005), which is defined as the difference in absorption of left-hand and right-hand circularly polarized light with optically active compounds.

Protein secondary structure can be determined by CD spectroscopy in the 'far-UV' spectral region (190–250 nm). At these wavelengths, the chromophore is the peptide bond, and the signal arises when it is located in a regular, folded environment (Kelly and Price, 1997). As determined, far-UV-CD of random coil is positive at 212 nm ($n \rightarrow \pi^*$) and negative at 195 nm ($\pi \rightarrow \pi^*$). Far-UV-CD of β-sheet is negative at 218 nm ($\pi \rightarrow \pi^*$) and positive at 196 nm ($n \rightarrow \pi^*$). For α-helix, the exciton coupling of the $\pi \rightarrow \pi^*$ transitions leads to positive ($\pi \rightarrow \pi^*$) perpendicular at 192 nm, negative ($\pi \rightarrow \pi^*$) parallel at 208 nm, and negative at 222 nm is red shifted ($n \rightarrow \pi^*$), respectively (Manavalan *et al.*, 1987; Kelly and Price, 1997). The approximate fraction of each secondary structure type that is present in any protein can thus be determined by analysing its far-UV CD spectrum as a sum of fractional multiples of such reference spectra for each structural type.

Secondary structures of wild-type and mutant Ugd were assessed by CD spectroscopy on an Aviv 62A DS CD spectrophotometer with a 1-mm path length cell, 0.5 nm wavelength step, and an averaging time of 3×10^{-1} s. The measurements were performed on 2.5 μM of protein in 10 mM Tris-HCl (pH 7.4). The CD spectra signals were collected from 195 nm to

260 nm at 25 °C and averaged over three scans (Coligan, 2003). The results were expressed as molar ellipticity, [θ] (degree cm^2 $dmol^{-1}$) which was determined as [θ] = (θ× 1000)/(*cl*), where *c* is the protein concentration in mmole/ml, *l* is the light path length in millimeters, and θ is the measured ellipticity in degrees at wavelength λ.

Software

Homology sequences were found from Protein database at NCBI (http://www.ncbi.nlm.nih.gov/) and alignment were performed with ClustalW2 program (Thompson *et al*., 1994) in EMBL-EBI (http://www.ebi.ac.uk/). The multiple alignments resulting from ClustalW analysis was used as input for BOXSHADE program (http://www.ch.embnet.org/software/ BOX form.html) to indicate residue similarity. The SWISS-MODEL (http://swissmodel.expasy.org/) comparative protein modeling server (Guex and Peitsch, 1997) was employed to generate a 3D model of the *Kp*Ugd protein based on the structural alignment of its sequence with the highest scoring template structure, with Pymol (http://www.pymol.org/) as a molecular viewer.

Construction of the specific *ugd*-deletion mutant

K. pneumoniae CG43 mutants disrupted specifically at *ugd* genes were constructed by the allelic exchange strategy. The primer sets used for PCR amplification of the DNA fragments flanking sequence are ugd001 and ugdM04 (Table 3). The generated DNA fragments were cloned into pKAS46, a suicide vector (a generous gift from Dr. Skorupski,

University of New Hampshire), and the resulting plasmids, pHY034, were then mobilized to *K. pneumoniae* CG43-S3 through conjugation from *E. coli* S17-1 λ *pir*. The transconjugants were selected with Ampicillin/Kanamycin on minimal medium (M9 minimal salts, Sigma). Some of the Ampicillin/Kanamycin resistant transconjugants was picked and then spread onto a LB plate supplemented with Streptomycin. When the occurrence of a double cross-over, the streptomycin-resistant and Ampicillin/Kanamycin-sensitive colonies were isolated, and the deletion of *ugd* was verified by PCR.

Construction of the Ugd and the UgdY71F-complemented strains

To obtain the complement of *ugd*, full length *ugd* including their promoter region was amplified from *K. pneumoniae* CG43-S3 with the primer pairs ugdNTUpo3 and ugdR (Table 3) and the DNA fragment was ligated into yT&A vector to generate yT&A-p*ugd*. The yT&A-p*ugd*Y71F was then constructed using QuikChange site-directed mutagenesis method (Stratagene). DNA fragments containing full length *ugd* with their promoter region were excised from yT&A-p*ugd* and yT&A-p*ugd*Y71F, respectively, with *Hind*III and *Xba*I. The DNA fragments were ligated respectively, into a *Hind*III/*Xba*I -digested plasmid pRK415, a broad host range plasmid (Keen *et al.*, 1998), to generate the *ugd* complementation plasmids, pRK415-p*ugd* and pRK415-p*ugd*Y71F.

Results

K. pneumoniae Ugd (*Kp*Ugd)

As shown in Fig. 1, alignment of the Ugd sequence of *K. pneumoniae* CG43 (Dr. S.-F Tsai, unpublished results), *E. coli* K-12 (NCBI accession No. NP_416532), *P. aeruginosa* PAO1 PA2022 (NCBI accession No. NP_250712) and PA3559 (NCBI accession No. NP_252249), and *B. subtilis* 168 (NCBI accession No. CAB15640) revealed that *Kp*Ugd and *Ec*Ugd, sharing 82% identity and 93% positives, are most closely related. The alignment also shows that, *Kp*Ugd contains a NAD^+ dinucleotide-binding domain, GXGXXG "fingerprint" of the Rossmann fold (Rossmann, 1981), at the N-terminal region and a nucleotide sugar-binding domain at the C-terminal part. In addition to the conserved signature of nucleotide sugar dehydrogenase, *Kp*Ugd also contains flanking sequence GG*X*C*XXX*D known to participate in catalysis. Finally, like the other Ugd, *Kp*Ugd contains an Arg at the position corresponding to Arg244 on *Sp*Ugd, which is one of the determinants of the substrate specificity of nucleotide sugar dehydrogenase (Campbell *et al*., 2000).

Selection for the phosphotyrosine residues on *Kp*Ugd

Recently, a *B. subtilis* phosphoproteome study reported that *Bs*Ugd was phosphorylated *in vivo* on a specific tyrosine residue Tyr70 (Macek *et al*., 2007). The counterpart residue Tyr 71of *Ec*Ugd was subsequently demonstrated to be the phosphorylation site by both tyrosine kinase *Ec*Wzc and *Ec*Etk. The phosphorylation of *Ec*Ugd-Tyr71 appeared to be essential for the Ugd activity as assessed using biological activity

complementation analysis (Lacour *et al*., 2008). Therefore, we assumed that the residue Tyr71 of *Kp*Ugd is also subject to phosphorylation.

Construction, expression and purification of the *Kp*Ugd mutants

In addition to Tyr71, 7 tyrosine residues of *Kp*Ugd (Y53, Y76, Y85, Y203, Y252, Y302, and Y380), which were not studied previously were selected for phenylalanine substitution (Fig. 1). After the site-specific substitution was confirmed by nucleotide sequencing, the mutant Ugd were cloned in pET-30b and expressed in *E. coli* NovaBlue (DE3), and the proteins purified through Ni^{+2}-NTA-agarose matrix. As shown in Fig. 2A, all the recombinant proteins could be overexpressed in *E. coli* NovaBlue (DE3). Most of the recombinant proteins appeared to be soluble and could be obtained in the supernatant fraction (Fig. 2B). In general, about 3.6 mg of Ugd and the derived mutant proteins of high purity (> 95%) could be obtained from a 100 ml culture (Fig. 2C). Interestingly, the IPTG-induced total protein lysates of pET-UgdY71F was less soluble compared to the others. Thus, about 500 ml cultured cells is needed to produce 2 mg of UgdY71F.

***In vivo* phosphorylation of the mutants with a substitution at a tyrosine residue**

To avoid the use of radioactive isotope for the detection of the phosphorylation reaction, we used anti-phosphotyrosine monoclonal antibody 4G10 (Fig. 3A) or Pro-Q® Diamond Phosphoprotein fluorescent dye (Fig. 3B) instead. It has been shown that *Ec*Wzc is able to

phosphorylate Ugd (Grangeasse *et al*., 2003). We have also shown that *Ec*Wzc could phosphorylate *Kp*Ugd (Appendix 4), and the recombinant Ugd purified from *E. coli* has been phosphorylated (Zhi-Kai Li, 2006). As shown in Fig. 3A or 3B, both *Kp*Wzc and *Kp*Ugd exhibited phosphorylation signals indicating phophatase has to be applied to remove the endogenous phosphorylation by *Ec*Wzc prior to the phosphorylation reaction.

In case that the phosphatase application may interfere the following phosphorylation, an *in vivo* phosphorylation without adding *Kp*Wzc was carried out to assess the tyrosine residue mutation effect on the *Kp*Ugd phosphorylation. As shown in Fig. 4, either the UgdWT or the derived site-specific mutants exhibited a phosphosignal of 46 kDa indicating none of the tyrosine mutation impaired the phosphorylation of *Kp*Ugd by *Ec*Wzc.

Determination of kinetic parameters of the UgdWT and the derived mutants

The initial velocity of the reaction by measuring the NADH absorbance at 340 nm was determined. As shown in Fig. 5, most of the mutant proteins (UgdY53F, UgdY71F, UgdY76F, UgdY203F, and UgdY302F) except Y85F, Y252F and Y380F mutants, when subjected to an enzyme specific activity measurement, performed just like the wild type. The specific activity of UgdY85F decreased to 0.49-fold, UgdY380F to 0.66-fold and UgdY252F to 0.15-fold of that of the UgdWT (Fig. 5).

Typical Lineweaver-Burk plots were obtained when 1/[v] was plotted against 1/[S]. Kinetic parameters, K_m and V_{max}, were estimated by linear regression from Lineweaver-Burk plots. The V_{max} values were converted to k_{cat} by assuming that the molar mass was 49416.38 g·mol $^{-1}$. The kinetic constants of His_6-tagged wild-type and mutant forms of Ugd for NAD^+ were calculated by fixing the concentration of UDP-glc with various concentrations of NAD^+ (Fig. 6). On the other hand, varying the concentration of UDP-glc with a constant concentration of NAD^+ was also used to measure the activity (Fig. 7).

As summarized in Table 4, the Ugd mutants (Y71F, Y252F and Y380F) could not efficiently utilize UDP-Glc and NAD^+ as demonstrated by the K_m and k_{cat} values. Interestingly, the specific activity obtained for UgdY71F was similar to that of wild-type. Moreover, the Y71F mutation had moderate effects on the kinetics of catalysis (15.4- and 10.3-fold above K_m values using UDP-glc and NAD^+ as substrates). The Y252F Ugd mutant exhibited undetectable K_m values to UDP-glc and NAD^+, while Y380F showed undetectable K_m values to UDP-glc but 3.5-fold increase of K_m values to NAD^+. The k_{cat} value of UgdY85F, Y252F orY380F for UDP-glc was much lower than that of the wild type Ugd. For NAD^+, the k_{cat} value of UgdY85F was slightly decreased (0.69-fold of wild type) while undetectable in Y262F.

Secondary structure analyses of Ugd and the derived mutants according to the circular dichroism spectrum.

After a modification (chemically／genetically) on specific protein,

CD can be a good technique to compare between native and modified forms (Tafreshi *et al*., 2007; Hadizadeh *et al*., 2007). The CD spectra were therefore used as a measure of the relative quantities of changes made in the derived mutants by site-directed mutagenesis.

As shown in Fig. 8, the far UV CD spectra of Y71F, Y85F, Y252F, Y380F and wild-type Ugd in Tris-HCl (pH 7.4) appeared to be identical and all showing a 'w'-shaped spectra with minimum point at 208 nm and 222 nm indicated the presence of high α-helix. This revealed that there is no major alteration of the secondary structures of the mutant proteins.

Structure modeling of *Kp*Ugd

The *Streptococcus pyogenes* Ugd (*Sp*Ugd) molecular structure has been solved and reported previously (Campbell *et al*., 2000). On the basis of homology (54.2% identity), comparative structural modeling was used to predict three-dimensional structure for *Kp*Ugd using the structure of *Sp*Ugd (PDB ID: 1DLIA) (Fig. 9A) as a template. By superimposing the context of the Ugd crystal structure of *S. pyogenes*, Cys253 in *Kp*Ugd was found at the position equivalent to catalytic nucleophile Cys260 in *Sp*Ugd (Fig. 9B).

Characterization of *Kp*Ugd deletion mutant

The *ugd* gene-specific deletion strain was constructed using the allelic exchange strategy to determine the functional roles of Ugd in *K. pneumoniae* physiology. As shown in Fig. 10A, the specific deletion was confirmed by PCR analysis. The Ugd deletion conferred *K. pneumoniae*

CG43 a change of morphotype from mucoid, fatty and shiny appearance to small and dull colonies (Fig. 10B). As assessed by the sedimentation assay shown in Fig. 10C, the *ugd* mutant appeared to be more readily precipitated via centrifugation in comparing with the wild type CG43-S3 suggesting the deletion of *ugd* reduced the synthesis of CPS.

However, introducing the complementation plasmids pRK415-Ugd or pET30b-Ugd (Fig. 11) into the *ugd* deletion mutant failed to restore the phenotype. The possibility that an impaired Ugd expression in the *ugd* mutant could be verified using pQE30 expression vector in the future.

Discussion

_Kp_Ugd has more than one tyrosine-phosporylation residue.

Capsular polysaccharide biosynthesis is controlled by phosphorylation at two levels: the assembly and export of the CPS (Wzc phosphorylation) and the synthesis of the CPS repeat unit (Ugd phosphorylation). We have previously established that Wzc-mediated phosphorylation of Ugd of *K. pneumoniae* CG43 influences the production of UDP sugar, the precursor for the bacterial CPS production. We have also shown that the phosphorylation of Ugd resulted in a significant increase of its dehydrogenase activity and the dephosphorylation by CIAP reduced its enzyme activity.

In order to identify the specific phosphotyrosine residue, nine of the 17 tyrosine residues have been chosen for site-directed mutagenesis study previously (Mei-Ju Li, 2008). However, all the Ugd site-directed mutants as well as the wild-type protein were phosphorylated by *Kp*Wzc, indicating the specific phosphoylation tyrosine residue on *Kp*Ugd has not yet identified. Here, an *in vivo* system to explore the tyrosine-phosphorylated residue of Ugd by *Ec*Wzc was used to avoid the interference of the CIAP treatment. Again, we found that all the mutants could be phosphorylated suggesting *Kp*Ugd has more than one tyrosine phosporylation site. The result is in agreement with the previous study showing that Ugd has multiple tyrosine phosphorylation sites detected by isotope autoradiography (Appendix 5).

The subject comes to identification of the second or third tyrosine residue. As shown in Appendix 5, the fragments GST-*Kp*Ugd2 (His68 to

Ala167) and GST-*Kp*Ugd3 (Glu168 to Gly300) showed intensive signals. Since Tyr71 is contained in GST-*Kp*Ugd2 (His68 to Ala167), we reason that the additional phosphotyrosine residue could be in GST-*Kp*Ugd3. Lacour and his co-workers have excluded the tyrosines Tyr10, Tyr150, Tyr249, Tyr335 and Tyr380 of *Ec*Ugd as phosphorylation site (Lacour *et al*., 2008). Thus, the Tyr252 of *Kp*Ugd of which the Phe replacement has caused changes of the kinetic properties was selected as the second phosphorylated site. The Ugd mutant with double site mutation (Tyr71 and Tyr252) will be generated to validate the hypothesis.

The Tyr residues participate in the *Kp*Ugd activity.

As reported by Mei-Ju Li (Mei-Ju Li, 2008), the activities of UgdY91F and UgdY210F were higher than that of the wild-type Ugd while UgdY10F, UgdY242F and UgdY249F exhibited a lower activity than that of the wild-type Ugd. In the study, three mutants with tyrosine to phenylalanine substitutions at positions 85, 252, and 380 had much lower activity than wild type. In addition, the k_{cat}/K_m value of UgdY71F, UgdY252F, and UgdY380F appeared much smaller than that of wild type. The single substitutions do not affect protein folding and have equivalent conformations as demonstrated via circular dichroism spectrum analysis. Tyr71 has been demonstrated as the phosphorylation site for *Ec*Ugd and Tyr70 for *Bs*Ugd. In analogy, we expected the purified UgdY71F would lose the phosphorlation signal and hence the enzyme activity. However, the tyrosine replacement only reduced slightly the k_{cat}/K_m value.

We speculate that the phosphorylation on Ugd adds a phosphate (PO_4)

molecule to a hydroxyl group of tyrosine residue that can turn a hydrophobic portion of a protein into a polar and extremely hydrophilic portion of molecule. In this way it introduces a conformational change via interaction with other hydrophobic and hydrophilic residues in the protein. Consequently, the entrance of catalytic pocket may be slightly moved to let the substrates contact the catalytic pocket more easily. The lower affinity to the substrates detected for UgdY71F may be due to the change of the phosphorylation state. This further supports the results of Appendix 2 that the phosphorylation of the Tyr71 of *Kp*Ugd plays a regulatory role for the enzymatic activity, which is different from the essential role of tyrosine phosphorylation on *Ec*Ugd.

The UDP-glc binding pocket can be divided into two regions: the UMP binding pocket composed solely of the residues from the C-terminal domain, and the glucose 1-phosphate binding pocket consisting primarily the residues from the N-terminal domain. The UMP binding pocket was lined with a stretch of coil (Tyr 242~Gly 250) that makes three main chain hydrogen bonds, two side chain hydrogen bonds, and a π-edge stacking interaction of Tyr242 with the UMP moiety. The glucose 1-phosphate binding pocket was found at the dimer interface, limited to a small region (Phe 142-Glu 145) between α7 and α8 of the N-terminal domain that forms three main hydrogen bonds to the glucose 1-phosphate moiety (Campbell *et al*., 2000). Nevertheless, Fig. 1 also revealed that central α-helix (α10) serving as the core of the dimer interface could be important. There are a total of 24 hydrogen bonds to stabilize the dimer interface, though none of the amino acids involved are strictly conserved.

The aromatic residues including Phe199, Tyr203, Tyr210, Tyr217, and Tyr265 were found to be located within the dimer interface.

On the basis of the structure modeling of *Kp*Ugd, Tyr85 is located beside the dimer interface and also close to the catalytic pocket. According to the enzymatic analysis, Y85F had effect on the specific activity, but not the kinetic properties. This suggested that Y85F may destroy the hydrogen bonds that stabilize the dimer interface without influencing the affinity between Ugd and substrates. The possibility could be verified using gel filtration chromatography to study whether a size difference is present between the preparation of Ugd and UgdY85F. Tyr252 is situated beside the catalytic site, Cys253, and very close to the interface of NAD^+ and UDP-glc which bound to the structurally pivotal active site of the enzyme. The activity abolished by substitution of Tyr252 to Phe may be attributed to the deletion of the phenolic hydroxyl group leading to impair the proton conductance pathway which in turn prevent from the oxidation of UDP-glc. Since Tyr380 was found to be strictly conserved among Ugds, if the alteration affects Ugd activity via influencing the binding to substrate or cofactor is unknown.

Overall, whether the altered enzymatic or kinetic effect is due to missing of the tyrosine phosphorylation or the change from tyrosine to phenylalanine *per se* remains to be investigated.

Bacterial tyrosine phosphorylation: novel targets for antibacterial therapy

The results provide a basis for understanding the regulatory

mechanism for biosynthesis of the CPS, a vital determinant for the initial stages of infection. Ugd has been considered as a crucial drug target for its critical role in EPS synthesis (Campbell *et al*., 2000). The kinetics study revealed some of the tyrosine residues are important for Ugd activity. Moreover, the presence of multiple tyrosine phosphorylation sites on *Kp*Ugd makes Ugd as a drug target more attractive. Further investigation on how Ugd affects drug susceptibility in bacteria may reveal new implications for future drug development.

Conclusion

To validate if *Kp*Ugd has more than one tyrosine-phosporylation residue, double-site mutations (Tyr71 and Tyr85, Tyr252, or Tyr380) or triple mutation will be generated. Phosphorylation assay and enzymatic measurement will then be performed to confirm the phosphorylation role of the tyrosine residues.

Reference

1. Alvarez, D., Merino, S., Tomas, J.M., Benedi, V.J., and Alberti, S. (2000) Capsular polysaccharide is a major complement resistance factor in lipopolysaccharide O side chain-deficient *Klebsiella pneumoniae* clinical isolates. *Infect Immun* **68**: 953-955.
2. Arakawa, Y., Wacharotayankun, R., Nagatsuka, T., Ito, H., Kato, N., and Ohta, M. (1995) Genomic organization of the *Klebsiella pneumoniae cps* region responsible for serotype K2 capsular polysaccharide synthesis in the virulent strain Chedid. *J Bacteriol* **177**: 1788-1796.
3. Bai, Ping-Hui (2004) Capsular polysaccharide production and protein-tyrosine phosphorylation in *Klebsiella pneumoniae* CG43. Master thesis, Department of Biological Science and Technology, National Chiao Tung University.
4. Binari RC, Staveley BE, Johnson WA, Godavarti R, Sasisekharan R, Manoukian AS. (1997) Genetic evidence that heparin-like glycosaminoglycans are involved in wingless signaling. *Development* **124(13)**:2623-32.
5. Breazeale SD, Ribeiro AA, Raetz CR. (2002) Oxidative decarboxylation of UDP-glucuronic acid in extracts of polymyxin-resistant Escherichia coli. Origin of lipid a species modified with 4-amino-4-deoxy-L-arabinose. *J Biol Chem* **277(4)**:2886-96.
6. Breazeale SD, Ribeiro AA, Raetz CR (2003) Origin of lipid A species modified with 4-amino-4-Deoxy-L-Arabinose in polymyxin resistant

mutants of Escherichia coli:An aminotransferase (ArnB) that generates UDP-4-amino-4-deoxy-Larabinose. *J Biol Chem* **278**: 24731–24739.

7. Brisse S, Grimont F, Grimont PAD (2006) The genus Klebsiella. In: Dworkin M, Falkow S, Rosenberg E, Schleifer K-H, Stackebrandt E, eds. The Prokaryotes ． A Handbook on the Biology of Bacteria. 3rd edition ed. New York: Springer.
8. Brisse S, Fevre C, Passet V, Issenhuth-Jeanjean S, Tournebize R, Diancourt L, Grimont P. (2009) Virulent clones of *Klebsiella pneumoniae*: identification and evolutionary scenario based on genomic and phenotypic characterization. *PLoS One* **4(3)**:e4982.
9. Brown, C. and R. J. Seidler (1973). "Potential pathogens in the environment: Klebsiella pneumoniae, a taxonomic and ecological enigma." *Appl Microbiol* **25(6)**: 900-4.
10. Campbell RE, Mosimann SC, van De Rijn I, Tanner ME, Strynadka NC. (2000)The first structure of UDP-glucose dehydrogenase reveals the catalytic residues necessary for the two-fold oxidation. *Biochemistry* **13;39(23)**:7012-23.
11. Chang, H.Y., Lee, J.H., Deng, W.L., Fu, T.F., and Peng, H.L. (1996) Virulence and outer membrane properties of a *galU* mutant of *Klebsiella pneumoniae* CG43. *Microb Pathog* **20**: 255-261.
12. Chien, HS (2008) ManC, Gnd and KpUgd are phosphorylated by tyrosine kinase, KpWzc of Klebsiella pneumoniae-Kinetic analysis of ManC and Gnd, identification of phosphotyrosine residues of KpUgd and search for other phosphorylation targe. Master thesis, Institute of

Molecular Medicine, National Tsing-Hua University.

13. Chou HC, Lee CZ, Ma LC, Fang CT, Chang SC, *et al*. (2004) Isolation of a chromosomal region of *Klebsiella pneumoniae* associated with allantoin metabolism and liver infection. *Infect Immun* **72**: 3783–3792.
14. Coligan, J.E. (2003) Current Protocols in Protein Science, John Wiley & Sons Inc., Brooklyn, NY, Unit 7.6.
15. Cozzone AJ (1998) Post-translational modification of proteins by reversible phosphorylation in prokaryotes. *Biochimie* **80**:43–48
16. Cozzone, A. J., Grangeasse C, Doublet P, Duclos B. (2004) Protein phosphorylation on tyrosine in bacteria. Arch *Microbiol* **181(3)**: 171–81
17. Cozzone, A. J. (2005) Role of protein phosphorylation on serine/threonine and tyrosine in the virulence of bacterial pathogens. *J Mol Microbiol Biotechnol* **9**, 198-213.
18. Cozzone, A. J. (2009) Bacterial tyrosine kinases: novel targets for antibacterial therapy? Trends *Microbiol* **17(12)**:536-43
19. Cross, A. S. (1990) Curr. Top. *Microbiol. Immunol.* **150**, 87–95
20. Dalessandro G, Northcote DH. (1977) Changes in enzymic activities of nucleoside diphosphate sugar interconversions during differentiation of cambium to xylem in sycamore and poplar. *Biochem J* **162(2)**:267-79.
21. Deutscher J, Francke C, Postma PW (2006) How phosphotransferase system-related protein phosphorylation regulates carbohydrate metabolism in bacteria. *Microbiol Mol Biol* Rev 70:939–1031

22. Doublet, P., Vincent, C., Grangeasse, C., Cozzone, A. J., and Duclos, B. (1999) On the binding of ATP to the autophosphorylating protein, Ptk, of the bacterium *Acinetobacter johnsonii*.*FEBS Lett* **445**, 137–143
23. Doublet, P., Grangeasse, C., Obadia, B., Vaganay, E., and Cozzone, A. J. (2002) Structural organization of the protein-tyrosine autokinase Wzc within *Escherichia coli* cells. *J. Biol. Chem* **277**, 37339–37348
24. Dutton GJ (1980) Acceptor substrates of UDP-glucuronosyltransferase and their assay, in Glucuronidation of Drugs and Other Compounds (Dutton GJ ed) pp 69–78, CRC Press, Boca Raton.
25. Fasman G.D. (1996) Circular Dichroism and the Conformational Analysis of Biomolecules. New York, USA: Plenum Publishing Corp.
26. Feingold, D. S. and Franzen, J. S. (1981). Pyridine nucleotide-linked four- electron transfer dehydrogenase. *Trends Biochem.* Sci. **6**, 103-105.
27. Fung, C. P., Chang, F. Y., Lee, S. C., Hu, B. S., Kuo, B. I., Liu, C. Y., Ho, M., and Siu, L. K. (2002) A global emerging disease of *Klebsiella pneumoniae* liver abscess: is serotype K1 an important factor for complicated endophthalmitis? *Gut* **50**, 420-424.
28. Grangeasse, C., Doublet, P., and Cozzone, A. J. (2002) Tyrosine phosphorylation of protein kinase Wzc from *Escherichia coli* K12 occurs through a two-step process. *J. Biol. Chem* **277**, 7127–7135
29. Grangeasse C, Obadia B, Mijakovic I, Deutscher J, Cozzone AJ, et al. (2003) Autophosphorylation of the *Escherichia coli* protein kinase Wzc regulates tyrosine phosphorylation of Ugd, a UDP-glucose dehydrogenase. *J Biol Chem* **278**: 39323–39329.

30. Grangeasse C, Cozzone AJ, Deutscher J, Mijakovie I. (2007) Tyrosine phosphorylation: an emerging regulatory device of bacterial physiology. *Trends Biochem* Sci. **32(2)**:86-94
31. Griffith, C. L., Klutts, J. S., Zhang, L., Levery, S. B., and Doering, T. L. (2004) *J. Biol. Chem* **279**, 51669–51676
32. Grimont PAD, Grimont F (2005) Genus *Klebsiella*. In: Brenner DJ, Krieg NR, Staley JT, eds. Bergey's manual of Systematic Bacteriology Volume 2: The Proteobacteria, Part B: The Gammaproteobacteria. New York: Springer-Verlag. pp 685–693.
33. Guex,N. and Peitsch,M.C. (1997) SWISS-MODEL and the Swiss-PdbViewer: an environment for comparative protein modeling. *Electrophoresis*, **18**, 2714-2723.
34. Hadizadeh Shirazy N., Ranjbar B., Hosseinkhani S., Khalifeh K., Riahi Madvar A., Naderi-Manesh H. (2007) Critical role of Glu175 on stability and folding of bacterial luciferase: stoppedflow fluorescence study. *J Biochem Mol Biol* **40**:453–458.
35. Hammes G.G. (2005) Spectroscopy for the Biological Sciences. New York, USA: John Wiley & Sons, Inc.
36. Hung RJ, Chien HS, Lin RZ, Lin CT, Vatsyayan J, Peng HL, Chang HY. Comparative analysis of two UDP-glucose dehydrogenases in *Pseudomonas aeruginosa* PAO1. *J Biol Chem* **282(24)**:17738-48.
37. Hunter T (2000) Signaling—2000 and beyond. *Cell* 100:113–127
38. Kelly S.M., Price N.C. (1997) The application of circular dichroism to studies of protein folding and unfolding. *Biochim Biophys Acta* **1338**:161–185.

39.Keen NT, Tamaki S, Kobayashi D, Trollinger D. (1998) Improved broad-host-range plasmids for DNA cloning in gram-negative bacteria. *Gene* **70(1)**:191-7

40.Kh. Tafreshi N., Hosseinkhani S., Sadeghizadeh M., Sadeghi M., Ranjbar B., Naderi-Manesh H. (2007) The influence of insertion of a critical residue (Arg356) in structure and bioluminescence spectra of firefly luciferase. *J Biol Chem* **282**:8641– 8647.

41.Klein G, Dartigalongue C, Raina S (2003) Phosphorylation-mediated regulation of heat shock response in *Escherichia coli*. *Mol Microbiol* **48**: 269–285.

42.Klumpp S, Krieglstein J (2002) Phosphorylation and dephosphorylation of histidine residues in proteins. *Eur J Biochem* **269**:1067–1071

43.Kohler JE, Hutchens MP, Sadow PM, Modi BP, Tavakkolizadeh A, et al. (2007) *Klebsiella pneumoniae* necrotizing fasciitis and septic arthritis: an appearance in the Western hemisphere. *Surg Infect* (Larchmt) **8**: 227–232.

44.Lacour S, Bechet E, Cozzone AJ, Mijakovic I, Grangeasse C. (2008) Tyrosine phosphorylation of the UDP-glucose dehydrogenase of Escherichia coli is at the crossroads of colanic acid synthesis and polymyxin resistance. *PLoS One* **3(8)**:e3053.

45.Lee DC, Zheng J, She YM, Jia Z (2008) Structure of *Escherichia coli* tyrosine kinase Etk reveals a novel activation mechanism. *EMBO J*.

46.Li, Zhi-Kai (2006) Functional analysis of the core elements, Wza, Yor5, Yco6 and Wzx, involved in capsular polysaccharide

biosynthesis in *Klebsiella pneumoniae* CG43. Master thesis, Department of Biological Science and Technology, National Chiao Tung University.

47. Li, Mei-Ju (2008) Identification of the phosphotyrosine residues in UDP-glucose dehydrogenase of *Klebsiella pneumoniae* CG43. Master thesis, Department of Bioengineering, National Chiao Tung University.

48. Lin MH, Hsu TL, Lin SY, Pan YJ, Jan JT, Wang JT, Khoo KH, Wu SH. (2009) Phosphoproteomics of *Klebsiella pneumoniae* NTUH-K2044 reveals a tight link between tyrosine phosphorylation and virulence. *Mol Cell Proteomics* **8**: 2613-2623

49. Lu CH, Chang WN, Chang HW (2002) *Klebsiella* meningitis in adults: clinical features, prognostic factors and therapeutic outcomes. *J Clin Neuro* sci **9**: 533–538.

50. Ma LC, Fang CT, Lee CZ, Shun CT, Wang JT (2005) Genomic heterogeneity in *Klebsiella pneumoniae* strains is associated with primary pyogenic liver abscess and metastatic infection. *J Infect Dis* **192**: 117–128.

51. Macek B, Mijakovic I, Olsen J, Gnad F, Kumar C, *et al*. (2006) Deciphering the prokaryotic Ser/Thre/Tyr phosphoproteome: the case of *Bacillus subtilis*. Seattle, WA, USA.

52. Macek B, Mijakovic I, Olsen JV, Gnad F, Kumar C, *et al*. (2007) The serine/threonine/tyrosine phosphoproteome of the model bacterium *Bacillus subtilis*. *Mol Cell Proteomics* **4**: 697–707.

53. Macek B, Gnad F, Soufi B, Kumar C, Olsen JV, *et al*. (2008)

Phosphoproteome analysis of E. coli reveals evolutionary conservation of bacterial Ser/Thr/Tyr phosphorylation. *Mol Cell Proteomics* **7**: 299–307.

54. Mijakovic, I., Poncet, S., Boel, G., Maze, A., Gillet, S., Jamet, E., Decottignies, P., Grangeasse, C., Doublet, P., Le Marechal, P., and Deutscher, J. (2003) Transmembrane modulator-dependent bacterial tyrosine kinase activates UDP-glucose dehydrogenases. *EMBO J* **22**: 4709-4718.
55. Mijakovic I, Petranovic D, Deutscher J (2004) How tyrosine phosphorylation affects the UDP-glucose dehydrogenase activity of *Bacillus subtilis* YwqF. *J Mol Microbiol Biotechnol* **8**: 19–25.
56. Mijakovic I, Petranovic D, Macek B, Cepo T, Mann M, et al. (2006) Bacterial single-stranded DNA-binding proteins are phosphorylated on tyrosine. *Nucleic Acids* Res **34**: 1588–1596.
57. Minic Z, Marie C, Delorme C, Faurie JM, Mercier G, et al. (2007) Control of EpsE, the phosphoglycosyltransferase initiating exopolysaccharide synthesis in *Streptococcus thermophilus*, by EpsD tyrosine kinase. *J Bacteriol* **189**: 1351–1357.
58. Mizuta, K., Ohta, M., Mori, M., Hasegawa, T., Nakashima, I., and Kato, N. (1983) Virulence for mice of *Klebsiella* strains belonging to the O1 group: relationship to their capsular (K) types. *Infect Immun* **40**, 56-61.
59. Mouslim, C., and E. A. Groisman. 2003. Control of the *Salmonella ugd* gene by three two-component regulatory systems. *Mol. Microbiol.* **47**:335-344.

60. Mouslim, C., T. Latifi, and E. A. Groisman. 2003. Signal-dependent requirement for the co-activator protein RcsA in transcription of the RcsB-regulated *ugd* gene. *J. Biol. Chem.* **278**:50588-50595.
61. Moxon, E. R., and Kroll, J. S. (1990) The role of bacterial polysaccharide capsules as virulence factors. Curr. Top. *Microbiol. Immunol.* **150**,65–85
62. Olivares-Illana V,Meyer P, Bechet E, Gueguen-Chaignon V, Lazereg-Riquier S, et al. (2008) Structural basis for the regulation mechanism of the tyrosine kinase CapB from *Staphylococcus aureus*. *PloS Biol.*
63. I. Ørskov and F. Ørskov, Serotyping of *Klebsiella*, *Methods Microbiol* **14** (1984), pp. 143–164.
64. Pawson T, Scott JD (2005) Protein phosphorylation in signaling—50 years and counting. *Trends Biochem* Sci **30**:286–290
65. Podschun, R., and Ullmann, U. (1998) *Klebsiella* spp. as nosocomial pathogens: epidemiology, taxonomy, typing methods, and pathogenicity factors. *Clin Microbiol Rev* **11**: 589-603.
66. Preneta, R., Jarraud, S., Vincent, C., Doublet, P., Duclos, B., Etienne, J., and Cozzone, A.J. (2002) Isolation and characterization of a protein-tyrosine kinase and a phosphotyrosine-protein phosphatase from *Klebsiella pneumoniae*. *Comp Biochem Physiol B Biochem Mol Biol* **131**: 103-112.
67. Rahn, A., Drummelsmith, J., and Whitfield, C. (1999) Conserved organization in the *cps* gene clusters for expression of *Escherichia coli* group 1 K antigens: relationship to the colanic acid biosynthesis locus

and the cps genes from *Klebsiella pneumoniae*. *J Bacteriol* **181**: 2307-2313.

68. Rahn, A., Beis, K., Naismith, J.H., and Whitfield, C. (2003) A novel outer membrane protein, Wzi, is involved in surface assembly of the *Escherichia coli* K30 group 1 capsule. *J Bacteriol* **185**: 5882-5890.
69. Ravichandran A, Sugiyama N, Tomita M, Swarup S, Ishihama Y. (2009) Ser/Thr/Tyr phosphoproteome analysis of pathogenic and non-pathogenic *Pseudomonas* species. *Proteomics* **9**, 1–12
70. Regue M, Climent N, Abitiu N, Coderch N, Merino S, et al. (2001) Genetic characterization of the *Klebsiella pneumoniae* waa gene cluster, involved in core lipopolysaccharide biosynthesis. *J Bacteriol* **183**: 3564–3573.
71. Roden. L. (1980). Structure and metabolism of connective tissue proteoglycans. In The Biochemistry of Glycoproteins and Proteoglycans (Ed. Lennarz. W. J.). pp 267-371, Plenum Publishing Co., New York.
72. Rossman MG. (1981) Evolution of glycolytic enzymes. *Philos Trans R Soc Lond B Biol Sci.* 26;**293(1063)**:191-203.
73. Seidler, R. J., M. D. Knittel, et al. (1975) Potential pathogens in the environment: cultural reactions and nucleic acid studies on *Klebsiella pneumoniae* from clinical and environmental sources. *Appl Microbiol* **29(6)**: 819-25.
74. Seifert, G. J. (2004) Nucleotide sugar interconversions and cell wall biosynthesis: how to bring the inside to the outside. Curr. Opin. *Plant Biol.* **7**, 277–284

75. Shi L, Potts M, Kennelly PJ (1998) The serine, threonine, and/or tyrosine-specific protein kinases and protein phosphatases of prokaryotic organisms: a family portrait. *FEMS Microbiol* Rev **22**:229–253

76. Simoons-Smit, A.M., Verweij-van Vught, A.M., and MacLaren, D.M. (1986) The role of K antigens as virulence factors in *Klebsiella*. *J Med Microbiol* **21**: 133-137.

77. Skorupski K., and Taylor RK. (1996) Positive selection vectors for allelic exchange. *Gene* **169(1)**:47-52

78. Soldo B, Lazarevic V, Pagni M, Karamata D. (1999) Teichuronic acid operon of *Bacillus subtilis* 168. *Mol. Microbiol.* **31(3)**:795-805

79. Soufi B, Gnad F, Jensen PR, Petranovic D, Mann M, Mijakovic I, Macek B. (2008) The Ser/Thr/Tyr phosphoproteome of *Lactococcus lactis* IL1403 reveals mutiply phosphorylated proteins. *Proteomics* **8**, 3486–3492

80. Soulat D, Grangeasse C, Vaganay E, Cozzone AJ, Duclos B (2007) UDP-acetylmannosamine dehydrogenase is an endogenous protein substrate of Staphylococcus aureus protein-tyrosine kinase activity. *J MolMicrobiol Biotechnol* **13**: 45–54.

81. Stevenson G, Andrianopoulos K, Hobbs M, Reeves PR (1996) Organization of the Escherichia coli K-12 gene cluster responsible for production of the extracellular polysaccharide colanic acid. *J Bacteriol* **178**: 4885–4893.

82. Sun X, Ge F, Xiao CL, Yin XF, Ge R, Zhang LH, He QY. (2010) Phosphoproteomic analysis reveals the multiple roles of

phosphorylation in pathogenic bacterium *Streptococcus pneumoniae*. *J Proteome* **9(1)**:275-82.

83. Thompson,J.D., Higgins,D.G. and Gibson,T.J. (1994) CLUSTAL W: improving the sensitivity of progressive multiple sequence alignment through sequence weighting, position-speci®c gap penalties and weight matrix choice. *Nucleic Acids* Res., **22**, 4673-4680.
84. Wacharotayankun, R., Arakawa, Y., Ohta, M., Hasegawa, T., Mori, M., Horii, T., and Kato, N. (1992) Involvement of *rcsB* in *Klebsiella* K2 capsule synthesis in *Escherichia coli* K-12. *J Bacteriol* **174**: 1063-1067.
85. Watson, D. A., and Musher, D. M. (1990) Interruption of capsule production in *Streptococcus pneumonia* serotype 3 by insertion of transposon Tn916. *Infect. Immun.* **58**, 3135–3138
86. Wessels, M. R., Goldberg, J. B., Moses, A. E., and DiCesare, T. J. (1994) Effects on virulence of mutations in a locus essential for hyaluronic acid capsule expression in group A streptococci. *Infect. Immun*. **62**, 433–441
87. Whitfield, C., and Roberts, I.S. (1999) Structure, assembly and regulation of expression of capsules in *Escherichia coli*. *Mol Microbiol* **31**: 1307-1319.
88. Whitfield, C. (2006) Biosynthesis and Assembly of Capsular Polysaccharides in *Escherichia coli*. *Annu Rev Biochem*.

Table I Bacterial strains used and constructed in this study

Strain	Genotype or relevant characteristic	Source or reference
E.coli:		
JM109	*RecA1 supE44 endA1 hsdR17 gyrA96 rolA1 thi* Δ*(lac-proAB)*	Laboratory stock
NovaBlue (DE3)	*endA1 hsdR17(rk12$^-$mk12$^+$) supE44 thi-1 recA1 gyrA96 relA1 lac*[F$'$ *pro AB lac^{q}Z*ΔM15:: Tn*10*](DE3);Tet^R	Novagen
BL21-RIL	*F$^-$ ompT hsdS$_B$(r$_B^-$m$_B^-$)gal dcm*(DE3)	Laboratory stock
S17-1 *λpir*	*RecA thi pro hsdR$^-$M$^+$* [RP4-2-Tc::Mu:Km^{R}Tn*7*] (*pir*)	De Lorenzo *et al*., 1994
K.pneumoniae:		
CG43	Clinical isolate of K2 serotype	Laboratory stock
CG43-S3	*rspL* mutant, Sm^R	Laboratory stock

Table II Plasmids used and constructed in this study

Plasmid	Description	Source or reference
yT&A	PCR cloning vector, Ap^R	Yeastern Biotech Co.
pKAS46	Suicide vector, *rspL*, Ap^R, Km^R	Skorupski and Taylor, 1996
pHY034	A 1685-bp fragment containing the flanking sequence of *ugd* cloned into pKAS46	Laboratory stock
pRK415	Broad-host-range IncP plasmid, Tc^R	Keen *et al*., 1998
pRK415-pUgd	*Kp*Ugd coding sequence with promoter region cloned in *Hin*dIII/*Xba*I sites, Km^R	This study
pRK415-pUgdY71F	pRK415-Ugd with single residue change of Ugd Y71F	This study
pET-30b	Overexpression of His6 fusion proteins, Km^R	Novagen
pET-*Kp*WzcE23	His_6–*Kp*Wzc(Arg^{451}-Lys^{722}) cloned in *Eco*RI/*Sal*I sites, Km^R	Zhi-Kai Li, 2005
pET-Ugd	His_6–*Kp*Ugd (Met^1 to Asp^{388}) cloned in *Eco*RI/*Sal*I sites, Km^R	Ping-Hui Bai, 2004
pET-UgdY53F	pET-Ugd with single residue change of Ugd Y53F	This study
pET-UgdY71F	pET-Ugd with single residue change of Ugd Y71F	This study

pET-UgdY76F	pET-Ugd with single residue change of Ugd Y76F	This study
pET-UgdY85F	pET-Ugd with single residue change of Ugd Y85F	This study
pET-UgdY203F	pET-Ugd with single residue change of Ugd Y203F	This study
pET-UgdY252F	pET-Ugd with single residue change of Ugd Y252F	This study
pET-UgdY302F	pET-Ugd with single residue change of Ugd Y302F	This study
pET-UgdY380F	pET-Ugd with single residue change of Ugd Y380F	This study

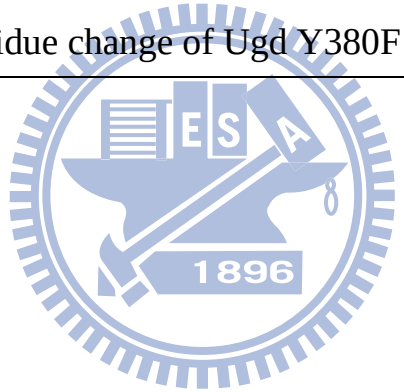

Table III Oligonucleotides used in this study

Primer	Sequence (5’ to 3’)
ugd001	GGCAAGAGCTCACCAGTGG
ugdM04	CATTACTTCCGCGACTTCG
ugdNTUpo3	GCAGGATCCATAATGGAAC
ugdR	TTAATCGTTACCAAACAGATCGCGGG
Y53FF	GATTCAGGAATTTCTGGCAGAAAAACC
Y53FR	GGTTTTTCTGCCAGAAATTCCTGAATC
Y71FF	GCACGACGCATTCCGTAATGCCGACTAC
Y71FR	GTAGTCGGCATTACGGAATGCGTCGTGC
Y76FF	CGTAATG CCGACTTCGT GATTATTGCC
Y76FR	GGCAATAATCACGAAGTCGGCATTACG
Y85FF	GCCGACCGACTTCGATCCCAAAACCAAC
Y85FR	GTTCGTTTTGGGATCGAAGTCGGTCGGC
Y203FF	GCT AACACCTTTC TGGCGCTGCG CGTTG
Y203FR	CAACGCCGCAGCGCCAGAAAGGTGTTAGC
Y252FF	CCTT TGGCTATGGC GGCTTCTGCC TGC
Y252FR	GCAGGCAGAAGCCGCCATAGCCAAAGG
Y302FF	GGTGGGTGTATTTCGCCTGATCATGAAG
Y302FR	CTTCATGATCAGGCGAAATACACCCACC
Y380FF	GA TAAGGTCTTCACCCGCGATCTGTTTG
Y380FR	CAAACAGATCGCGGGTGAAGACCTTATC

Table IV Kinetic parameters of UgdWT and the derived mutants

		K_m (mM)	V_{max} (mMmin^{-1})	k_{cat} (min^{-1})	k_{cat}/K_m (min^{-1}mM^{-1})
Ugd WT	UDP-glc	0.44±0.06	0.06±0.003	639.73±33.8	1472±254.66
	NAD^+	0.08±0.005	0.04±0.002	395.99±25.71	4961.82±653.82
Y53F	UDP-glc	1±0.09	0.12±0.005	1146.39±48.35	1148.2±58.19
	NAD^+	0.07±0.001	0.08±0.007	779.3±72.59	10170.05±974.8
Y71F	UDP-glc	6.76±0.57	0.24±0.03	2393.13±316.89	354.82±42.24
	NAD^+	0.82±0.09	0.06±0.02	589.14±183.81	705.61±145.89
Y76F	UDP-glc	0.34±0.06	0.07±0.01	705.5±107.57	2091.41±67.53
	NAD^+	0.07±0.006	0.07±0.008	667.22±79.51	10071.59±762.38
Y85F	UDP-glc	0.13±0.01	0.02±0.003	242.23±31.5	1918.35±106.85
	NAD^+	0.04±0.005	0.027±0.004	269.27±40.46	6089.23±721.3
Y203F	UDP-glc	0.64±0.09	0.08±0.015	759.23±143.29	1173.43±49.03
	NAD^+	0.1±0.013	0.04±0.002	380.96±17.52	3860.5±632.99
Y252F	UDP-glc	ND	ND	ND	ND
	NAD^+	ND	ND	ND	ND
Y302F	UDP-glc	0.47±0.07	0.08±0.012	747.69±121.09	1593.93±121.19
	NAD^+	0.07±0.005	0.007±0.008	662.67±83.35	9891.45±1201.14
Y380F	UDP-glc	ND	ND	ND	ND
	NAD^+	0.28±0.09	0.05±0.007	447.67±73.26	1719.21±710.3

[a] k_{cat} was calculated from the equation $V_{max} = k_{cat} \cdot$ [Eo], where Eo is the molar concentration of Ugd. The results are the average of three independent experiments.

[b] ND indicates not detected.

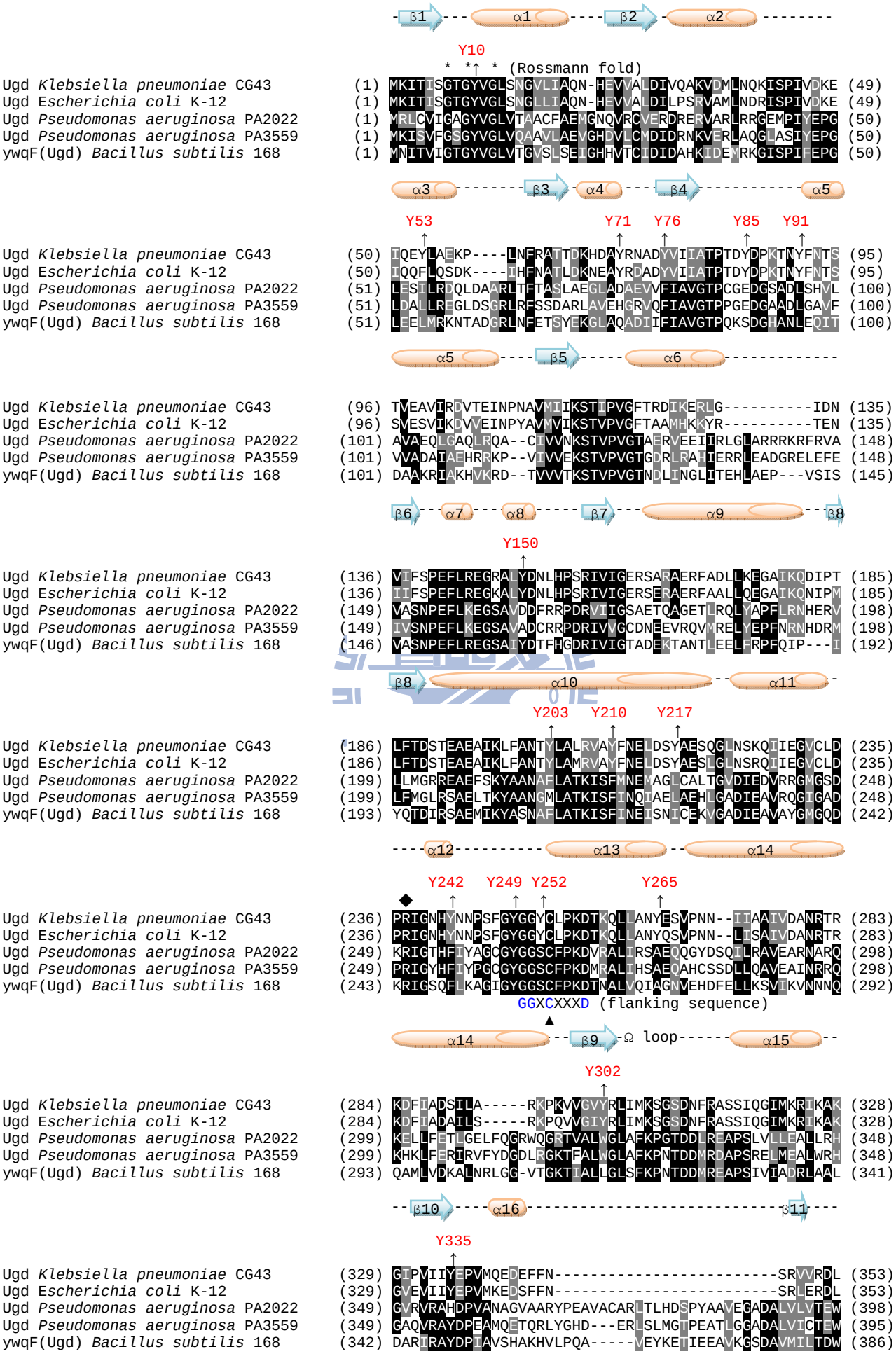
β1 α1 β2 α2
Y10
* *↑ * (Rossmann fold)
Ugd Klebsiella pneumoniae CG43 (1) MKITISGTGYVGLSNGVLIAQN-HEVVALDIVQAKVDMLNQKISPIVDKE (49)
Ugd Escherichia coli K-12 (1) MKITISGTGYVGLSNGLLIAQN-HEVVALDILPSRVAMLNDRISPIVDKE (49)
Ugd Pseudomonas aeruginosa PA2022 (1) MRLCVIGAGYVGLVTAACFAEMGNQVRCVERDRERVARLRRGEMPIYEPG (50)
Ugd Pseudomonas aeruginosa PA3559 (1) MKISVFGSGYVGLVQAAVLAEVGHDVLCMDIDRNKVERLAQGLASIYEPG (50)
ywqF(Ugd) Bacillus subtilis 168 (1) MNITVIGTGYVGLVTGVSLSEIGHHVTCIDIDAHKIDEMRKGISPIFEPG (50)
α3 β3 α4 β4 α5
Y53 Y71 Y76 Y85 Y91
Ugd Klebsiella pneumoniae CG43 (50) IQEYLAEKP----LNFRATTDKHDAYRNADYVIIATPTDYDPKTNYFNTS (95)
Ugd Escherichia coli K-12 (50) IQQFLQSDK----IHFNATLDKNEAYRDADYVIIATPTDYDPKTNYFNTS (95)
Ugd Pseudomonas aeruginosa PA2022 (51) LESILRDQLDAARLTFTASLAEGLADAEVVFIAVGTPCGEDGSADLSHVL (100)
Ugd Pseudomonas aeruginosa PA3559 (51) LDALLREGLDSGRLRFSSDARLAVEHGRVQFIAVGTPPGEDGAADLGAVF (100)
ywqF(Ugd) Bacillus subtilis 168 (51) LEELMRKNTADGRLNFETSYEKGLAQADIIFIAVGTPQKSDGHANLEQIT (100)
α5 β5 α6
Ugd Klebsiella pneumoniae CG43 (96) TVEAVIRDVTEINPNAVMIIKSTIPVGFTRDIKERLG----------IDN (135)
Ugd Escherichia coli K-12 (96) SVESVIKDVVEINPYAVMVIKSTVPVGFTAAMHKKYR----------TEN (135)
Ugd Pseudomonas aeruginosa PA2022 (101) AVAEQLGAQLFQA--CIVVNKSTVPVGTAERVEEIIRLGLARRRKRFRVA (148)
Ugd Pseudomonas aeruginosa PA3559 (101) VVADAIAEHRFKP--VIVVEKSTVPVGTGDRLRAFIERRLEADGRELEFE (148)
ywqF(Ugd) Bacillus subtilis 168 (101) DAAKRIAKHVKRD--TVVVTKSTVPVGTNDLINGLITEHLAEP---VSIS (145)
β6 α7 α8 β7 α9 β8
Y150
Ugd Klebsiella pneumoniae CG43 (136) VIFSPEFLREGRALYDNLHPSRIVIGERSARAERFADLLKEGAIKQDIPT (185)
Ugd Escherichia coli K-12 (136) IIFSPEFLREGKALYDNLHPSRIVIGERSERAERFAALLQEGAIKQNIPM (185)
Ugd Pseudomonas aeruginosa PA2022 (149) VASNPEFLKEGSAVDDFRRPDRVIIGSAETQAGETLRQLYAPFLRNHERV (198)
Ugd Pseudomonas aeruginosa PA3559 (149) IVSNPEFLKEGSAVADCRRPDRIVVGCDNEEVRQVMRELYEPFNRNHDRM (198)
ywqF(Ugd) Bacillus subtilis 168 (146) VASNPEFLREGSAIYDTFHGDRIVIGTADEKTANTLEELFRPFQIP---I (192)
β8 α10 α11
Y203 Y210 Y217
Ugd Klebsiella pneumoniae CG43 (186) LFTDSTEAEAIKLFANTYLALRVAYFNELDSYAESQGLNSKQIIEGVCLD (235)
Ugd Escherichia coli K-12 (186) LFTDSTEAEAIKLFANTYLAMRVAYFNELDSYAESLGLNSRQIIEGVCLD (235)
Ugd Pseudomonas aeruginosa PA2022 (199) LLMGRREAEFSKYAANAFLATKISFMNEMAGLCALTGVDIEDVRRGMGSD (248)
Ugd Pseudomonas aeruginosa PA3559 (199) LFMGLRSAELTKYAANGMLATKISFINQIAELAEHLGADIEAVRQGIGAD (248)
ywqF(Ugd) Bacillus subtilis 168 (193) YQTDIRSAEMIKYASNAFLATKISFINEISNICEKVGADIEAVAYGMGQD (242)
α12 α13 α14
Y242 Y249 Y252 Y265
Ugd Klebsiella pneumoniae CG43 (236) PRIGNHYNNPSFGYGGYCLPKDTKQLLANYESVPNN--IIAAIVDANRTR (283)
Ugd Escherichia coli K-12 (236) PRIGNHYNNPSFGYGGYCLPKDTKQLLANYQSVPNN--LISAIVDANRTR (283)
Ugd Pseudomonas aeruginosa PA2022 (249) KRIGTHFIYAGCGYGGSCFPKDVRALIRSAEQQGYDSQILRAVEARNARQ (298)
Ugd Pseudomonas aeruginosa PA3559 (249) PRIGYHFIYPGCGYGGSCFPKDMRALIHSAEQAHCSSDLLQAVEAINRRQ (298)
ywqF(Ugd) Bacillus subtilis 168 (243) KRIGSQFLKAGIGYGGSCFPKDTNALVQIAGNVEHDFELLKSVIKVNNQ (292)
GGXCXXXD (flanking sequence)
α14 β9 Ω loop α15
Y302
Ugd Klebsiella pneumoniae CG43 (284) KDFIADSILA-----RKPKVVGVYRLIMKSGSDNFRASSIQGIMKRIKAK (328)
Ugd Escherichia coli K-12 (284) KDFIADAILS-----RKPQVVGIYRLIMKSGSDNFRASSIQGIMKRIKAK (328)
Ugd Pseudomonas aeruginosa PA2022 (299) KELLFETLGELFQGRWQGRTVALWGLAFKPGTDDLREAPSLVLLEALLRH (348)
Ugd Pseudomonas aeruginosa PA3559 (299) KHKLFERIRVFYDGDLRGKTFALWGLAFKPNTDDMRDAPSRELMEALWRH (348)
ywqF(Ugd) Bacillus subtilis 168 (293) QAMLVDKALNRLGG-VTGKTIALLGLSFKPNTDDMREAPSIVIADRLAAL (341)
β10 α16 β11
Y335
Ugd Klebsiella pneumoniae CG43 (329) GIPVIIYEPVMQEDEFFN----------SRVVRDL (353)
Ugd Escherichia coli K-12 (329) GVEVIIYEPVMKEDSFFN----------SRLERDL (353)
Ugd Pseudomonas aeruginosa PA2022 (349) GVRVRAHDPVANAGVAARYPEAVACARLTLHDSPYAAVEGADALVLVTEW (398)
Ugd Pseudomonas aeruginosa PA3559 (349) GAQVRAYDPEAMQETQRLYGHD---ERLSLMGTPEATLGGADALVICTEW (395)
ywqF(Ugd) Bacillus subtilis 168 (342) DARIRAYDPIAVSHAKHVLPQA-----VEYKETIEEAVKGSDAVMILTDW (386)

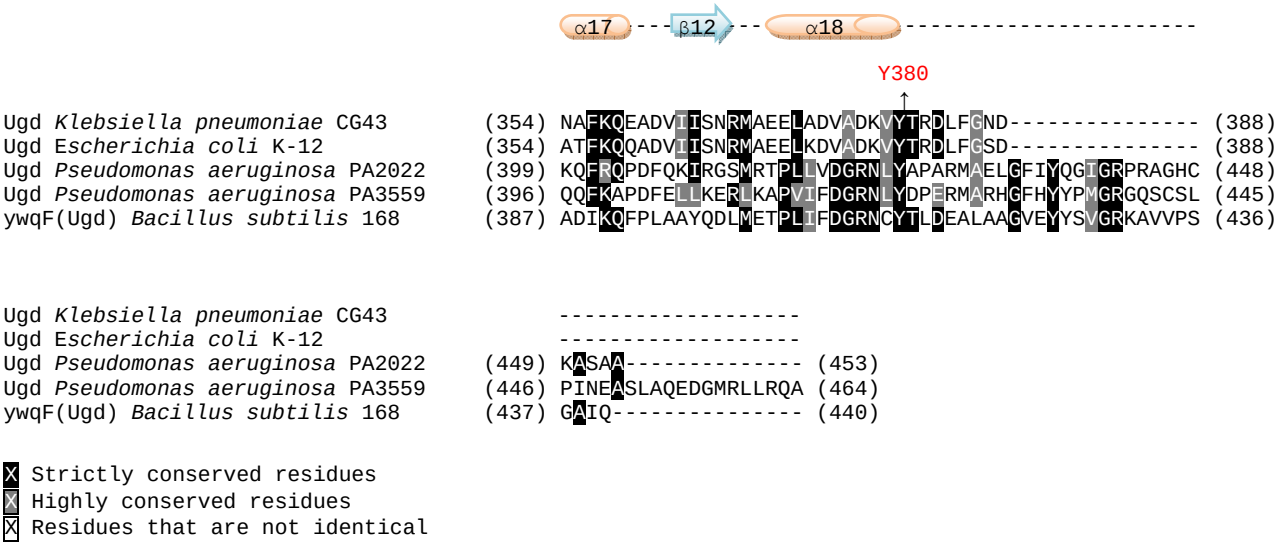

Fig. 1. Sequence comparison of Ugd from different bacteria. Multiple sequence alignment of Ugd from *K. pneumoniae*, *E. coli* K-12, *P. aeruginosa* PA2022, *P. aeruginosa* PA3559, and *B. subtilis* 168 is shown. The thin arrows point to the position of the mutated tyrosine residues. Among them, the eight tyrosine residues (Y53F, Y71F, Y76F, Y85F, Y203F, Y252F, Y302F and Y380F) were mutated in this study. The asterisks indicate the position of the Rossmann fold, which contains a consensus sequence GXGXXG (Rossmann, 1981). The arrowhead indicates the catalytic Cys253, with a flanking sequence of GGXCXXXD and the rhombus points to a residue that determines the substrate specificity of the enzymes (Campbell *et al*., 2000). Residues identical in at least three of the comparison sequences are highlighted. Secondary structural elements are shown schematically with cylinders representing α-helices and thick arrows representing β-strands.

A

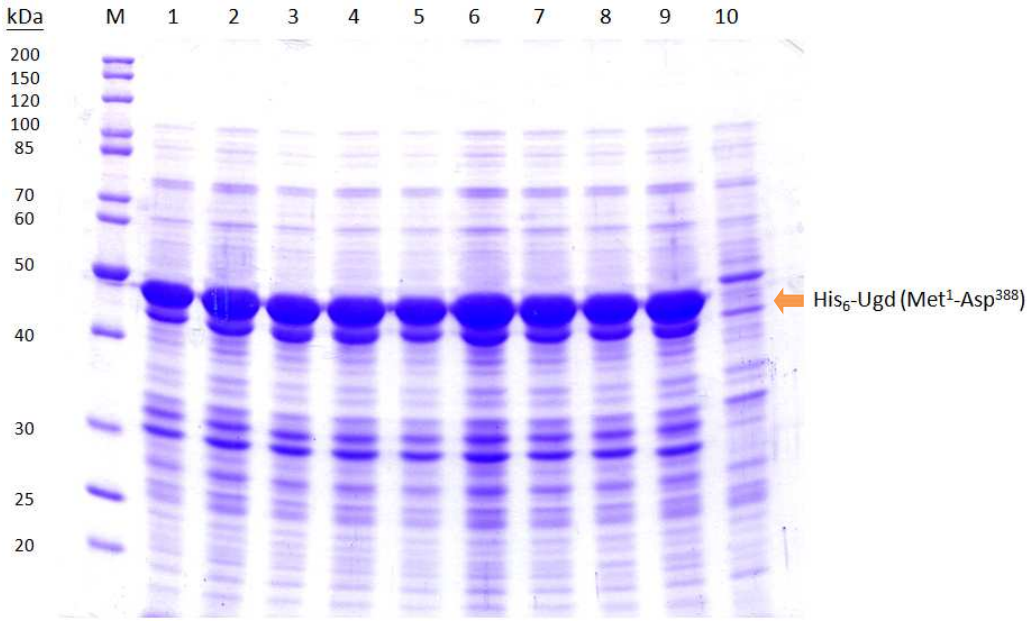
kDa
M
1
2
3
4
5
6
7
8
9
10
200
150
120
100
85
70
60
50
40
30
25
20
His6-Ugd (Met1-Asp388)

B

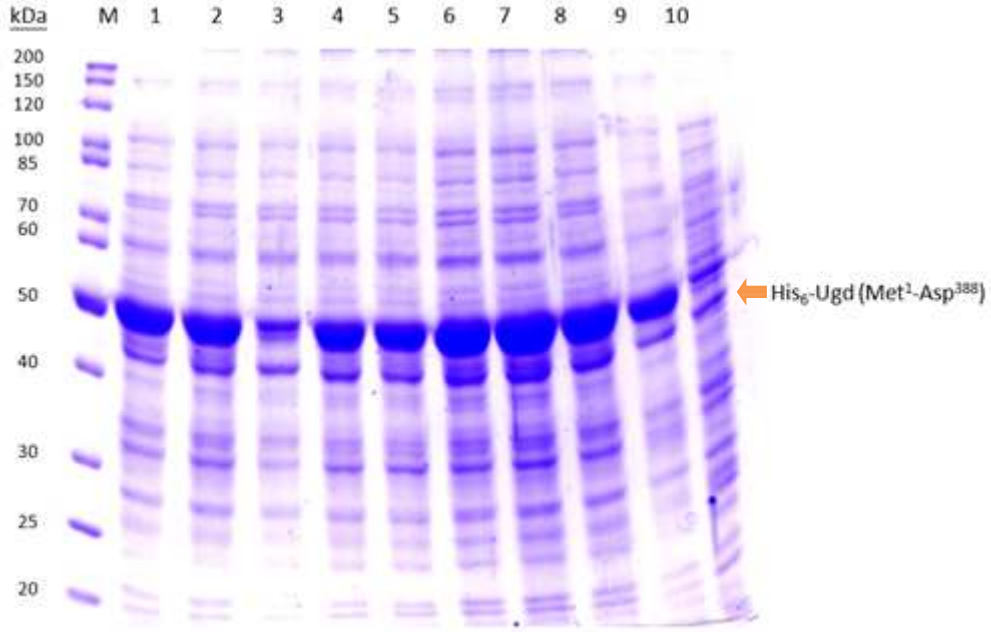
kDa
M
1
2
3
4
5
6
7
8
9
10
200
150
120
100
85
70
60
50
40
30
25
20
His6-Ugd (Met1-Asp388)

C

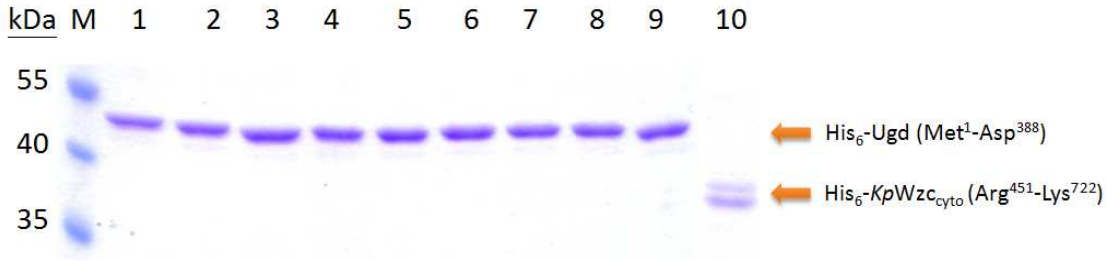

Fig.2. Expression and purification of the recombinant Ugd proteins. Total proteins isolated from the recombinant *E. coli* carrying each of the recombinant clones of pET-30b-Ugd or pET-30b-Wzc were subjected to SDS-PAGE and visualized by staining with Coomassie Brilliant Blue. Lane M: molecular weights standards. The molecular mass labeled in kDa is shown on the left. Lanes 1, Ugd WT; 2 to 9 are Ugd mutant proteins, Y53F, Y71F, Y76F, Y85F, Y203F, Y252F, Y302F, and Y380F respectively; Lane 10, Wzc. (A) total protein lysate, (B) supernatant, and (C) purified Ugd.

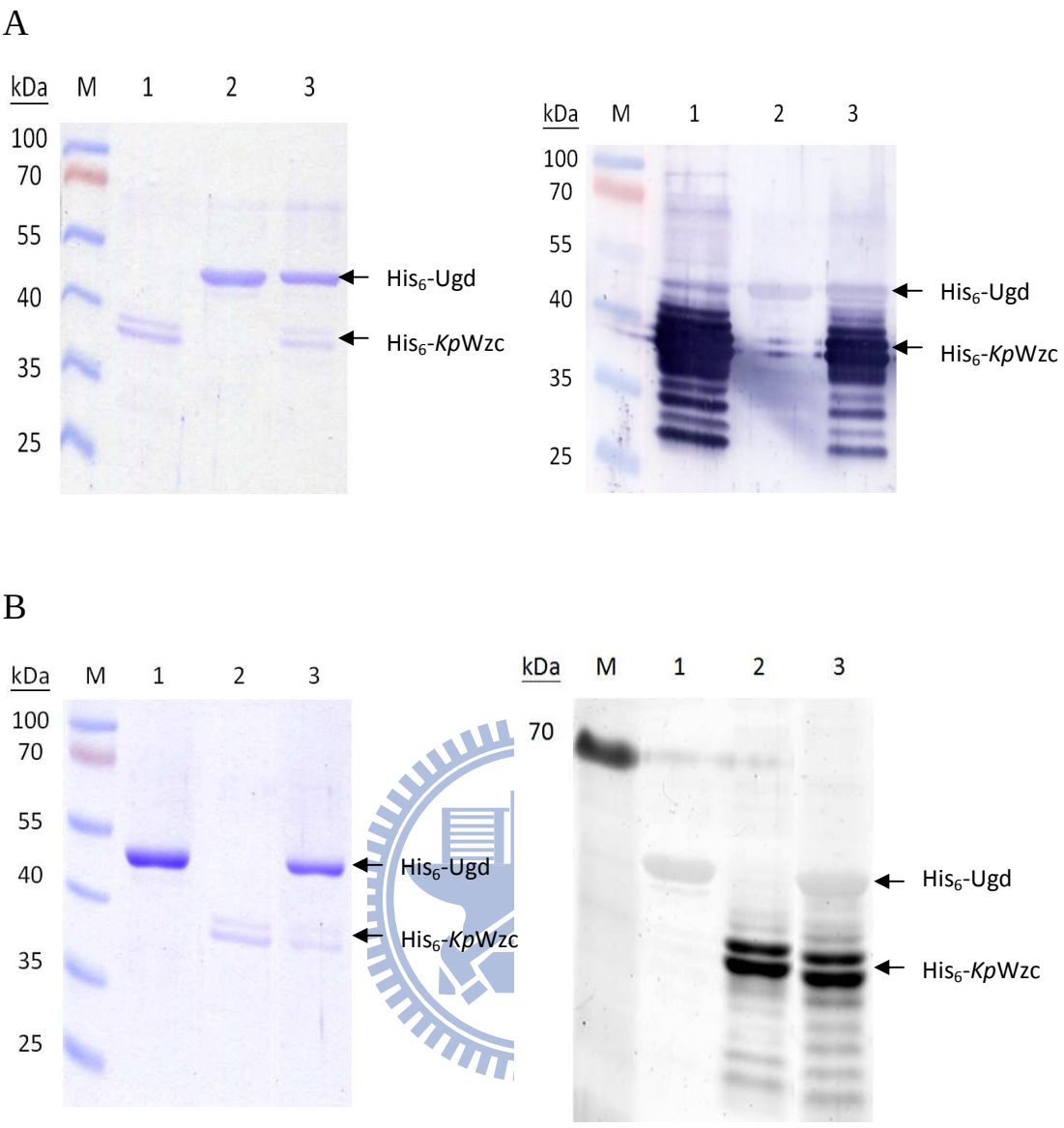

Fig.3. In vitro phosphorylation of Ugd. *In vitro* phosphorylation was performed in the presence of exogenously added *Kp*Wzc. The molecular weight markers are indicated on left. The gels were stained with Commassie Blue (left panel) and analyzed by (A) Western blot with 4G10 antibody: lane1 His_6-*Kp*Wzc; 2,Ugd WT; 3, His_6-*Kp*Wzc and Ugd WT; and (B) Pro-Q® Diamond Phosphoprotein fluorescent dye : lane1 Ugd WT; 2, His_6-*Kp*Wzc; 3, His_6-*Kp*Wzc and Ugd WT.

A

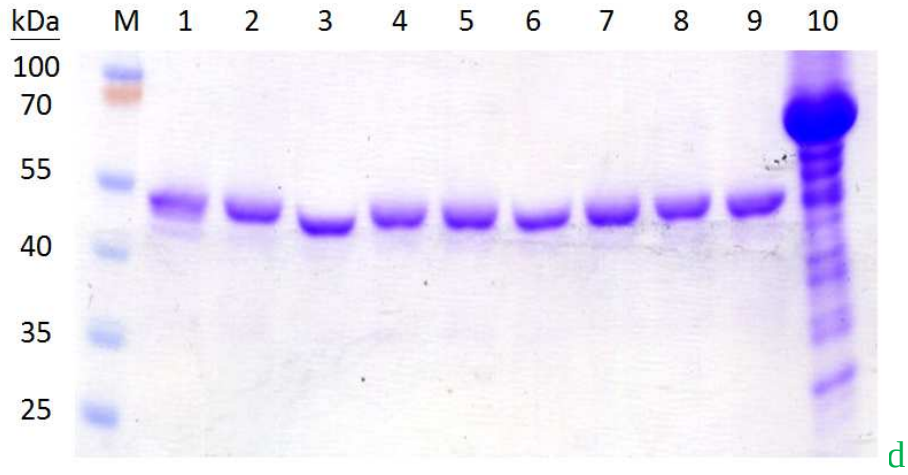

d

B

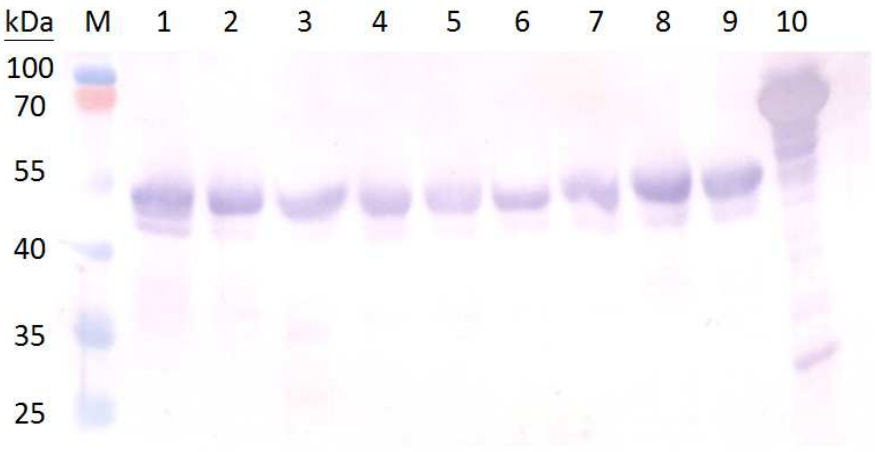

Fig. 4. In vivo phosphorylation of Ugd and the derived mutants. In vivo phosphorylation was performed in the presence of endogenously *E.coli* Wzc. (A) SDS-PAGE stained with Coomassie blue (B) Western Blot with anti-phosphotyrosine (clone 4G10) antibody. Lanes 1 Ugd WT; 2 to 9 are Ugd mutant proteins, Y53F, Y71F, Y76F, Y85F, Y203F, Y252F, Y302F, and Y380F, respectively; 10, bovine serum albumin (BSA), phosphorylated protein, as positive control of staining. The molecular weight markers are indicated on left.

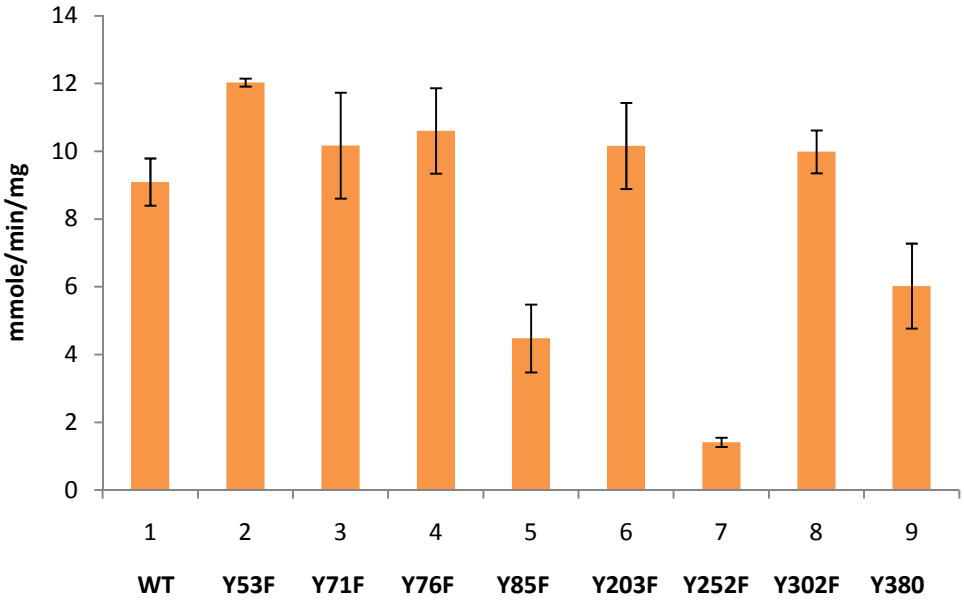

Fig. 5. Specific activity of the Ugd variants. The reaction mixture contains 100 mM Tris-HCl (pH 9.0), 100 mM NaCl, 2 mM DTT, 2 mM NAD^+ and 5 mM UDP-glc and Ugd or the Ugd mutant. UDP-glc was added after detecting 20 s, and the formation of NADH was detected at 340 nm.

A

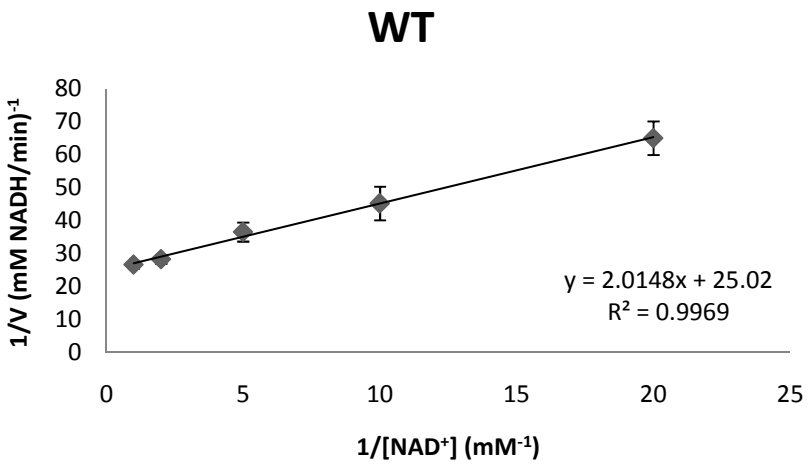
WT
1/V (mM NADH/min)-1
80
70
60
50
40
30
20
10
0
0
5
10
15
20
25
y = 2.0148x + 25.02
R² = 0.9969
1/[NAD+] (mM-1)

B

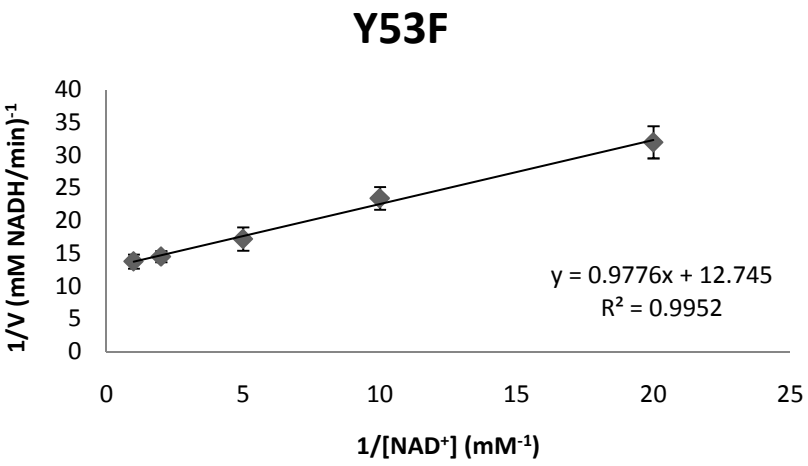
Y53F
1/V (mM NADH/min)-1
40
35
30
25
20
15
10
5
0
0
5
10
15
20
25
y = 0.9776x + 12.745
R² = 0.9952
1/[NAD+] (mM-1)

C

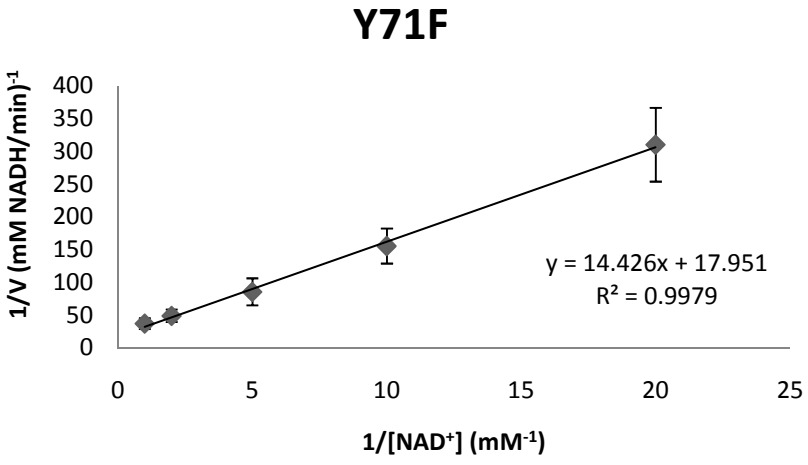
Y71F
1/V (mM NADH/min)-1
400
350
300
250
200
150
100
50
0
0
5
10
15
20
25
y = 14.426x + 17.951
R² = 0.9979
1/[NAD+] (mM-1)

D

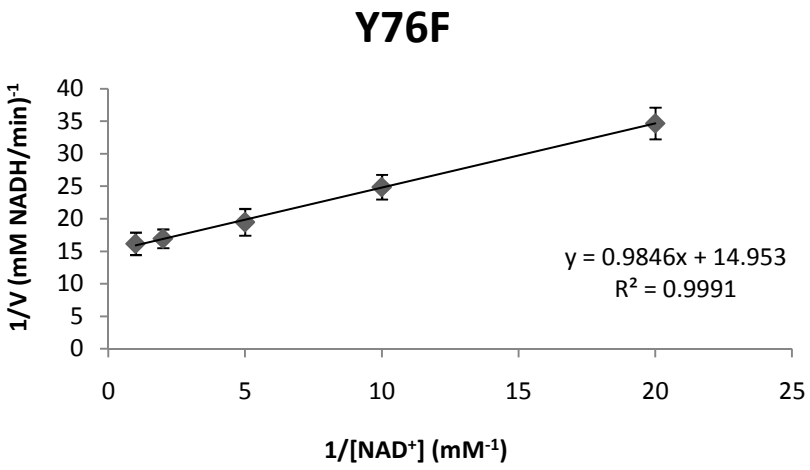
Y76F
1/V (mM NADH/min)-1
40
35
30
25
20
15
10
5
0
0
5
10
15
20
25
y = 0.9846x + 14.953
R² = 0.9991
1/[NAD+] (mM-1)

E

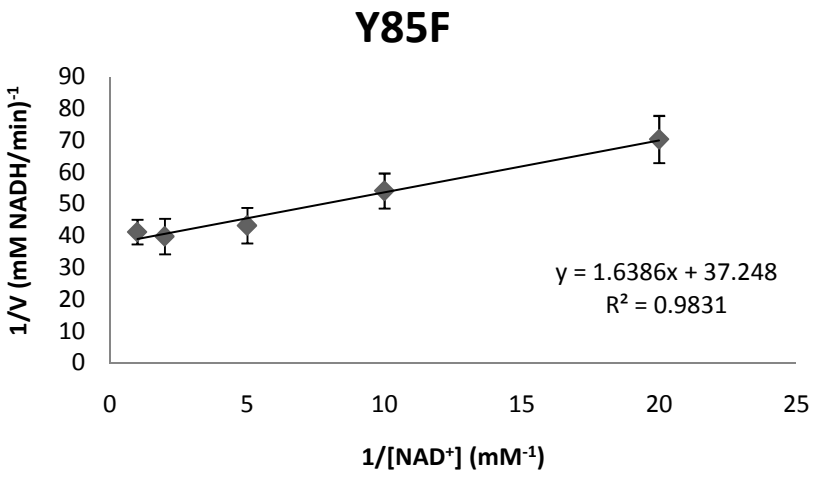
Y85F
1/V (mM NADH/min)-1
90
80
70
60
50
40
30
20
10
0
0
5
10
15
20
25
y = 1.6386x + 37.248
R² = 0.9831
1/[NAD+] (mM-1)

F

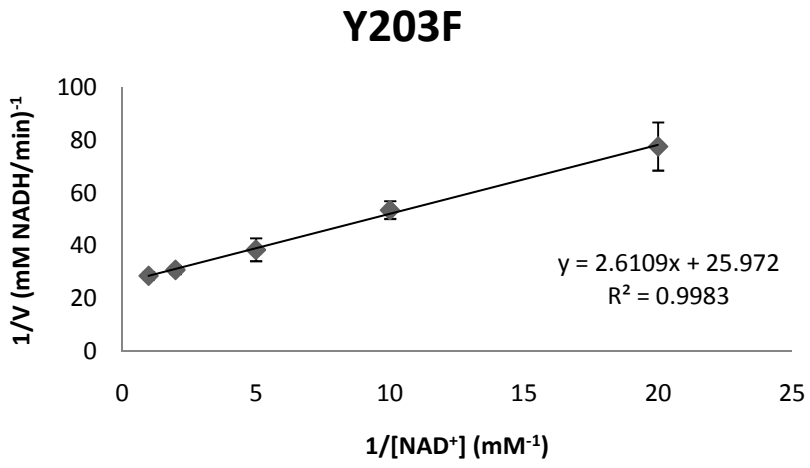
Y203F
1/V (mM NADH/min)-1
100
80
60
40
20
0
0
5
10
15
20
25
y = 2.6109x + 25.972
R² = 0.9983
1/[NAD+] (mM-1)

G

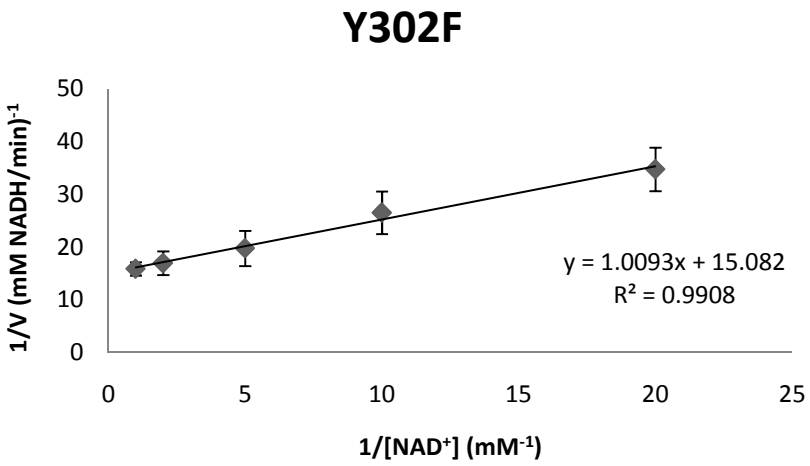

H

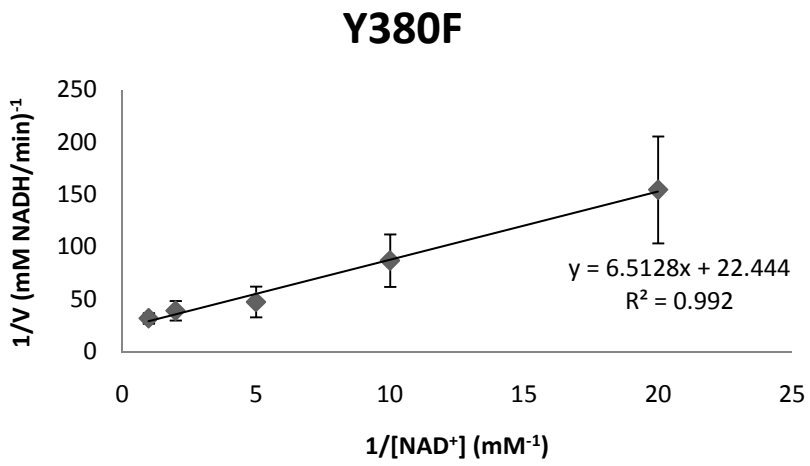

Fig. 6. Lineweaver–Burk plot of the wild type Ugd and its derivatives at five different concentration of NAD^+. The double reciprocal plot of the wild type Ugd and the derived mutants at five NAD^+ concentrations are shown. The intercept on the ordinate is equal to $1/V_{max}$, and the intercept on the abscissa is equal to $-1/K_m$. The data represent the mean ± SD of triplicate difference experiment. (A) Ugd WT, (B) Y53F, (C) Y71F, (D) Y76F, (E) Y85F, (F) Y203F, (G) Y302F, (H) Y380F

A

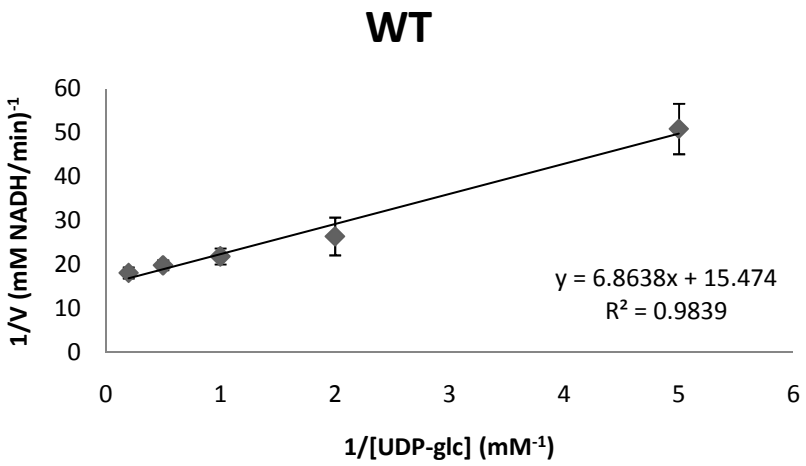
WT
1/V (mM NADH/min)-1
60
50
40
30
20
10
0
0
1
2
3
4
5
6
y = 6.8638x + 15.474
R² = 0.9839
1/[UDP-glc] (mM-1)

B

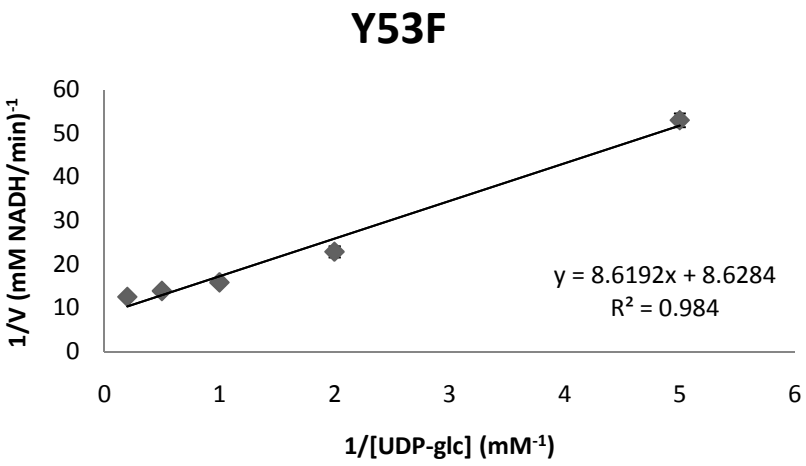
Y53F
1/V (mM NADH/min)-1
60
50
40
30
20
10
0
0
1
2
3
4
5
6
y = 8.6192x + 8.6284
R² = 0.984
1/[UDP-glc] (mM-1)

C

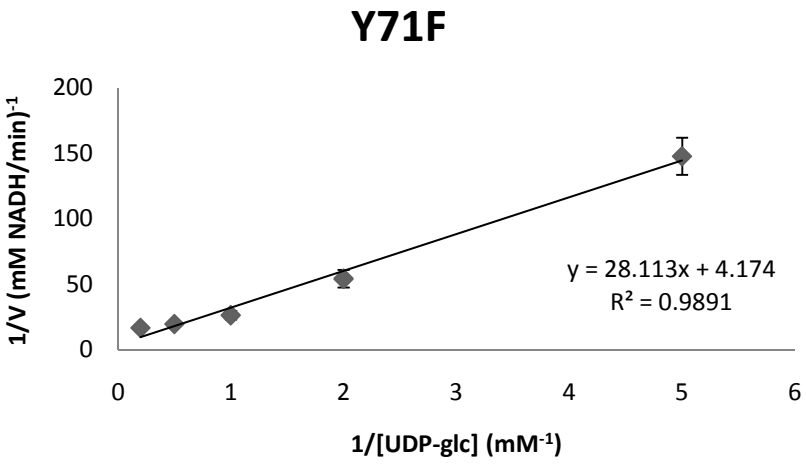
Y71F
1/V (mM NADH/min)-1
200
150
100
50
0
0
1
2
3
4
5
6
y = 28.113x + 4.174
R² = 0.9891
1/[UDP-glc] (mM-1)

D

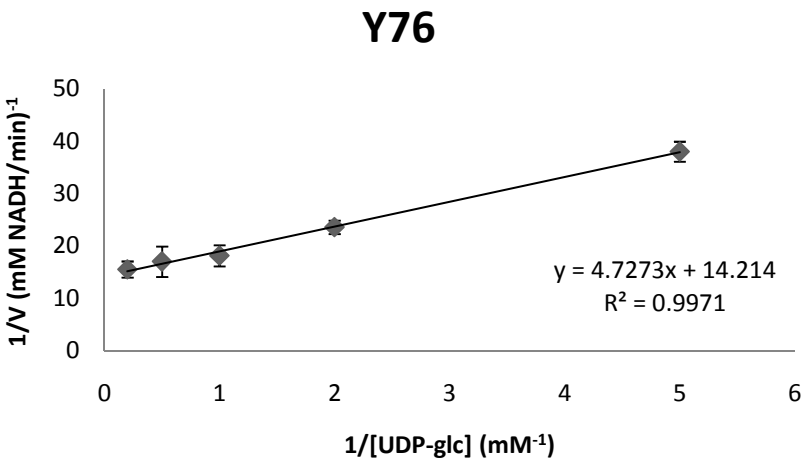
Y76
1/V (mM NADH/min)-1
50
40
30
20
10
0
0
1
2
3
4
5
6
1/[UDP-glc] (mM-1)
y = 4.7273x + 14.214
R² = 0.9971

E

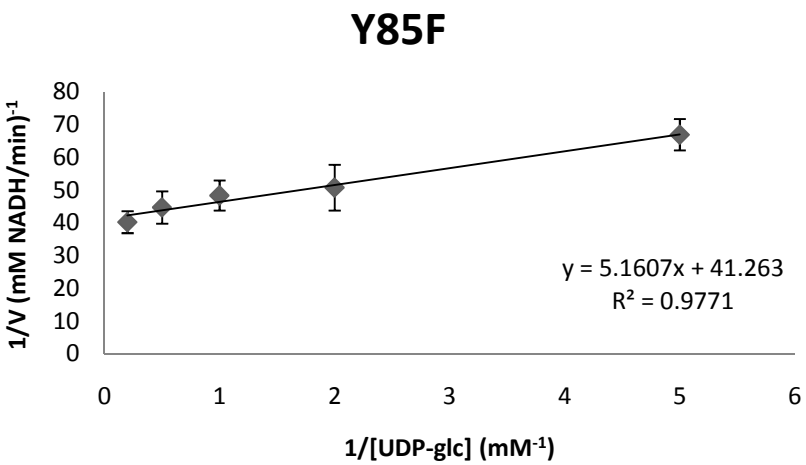
Y85F
1/V (mM NADH/min)-1
80
70
60
50
40
30
20
10
0
0
1
2
3
4
5
6
1/[UDP-glc] (mM-1)
y = 5.1607x + 41.263
R² = 0.9771

F

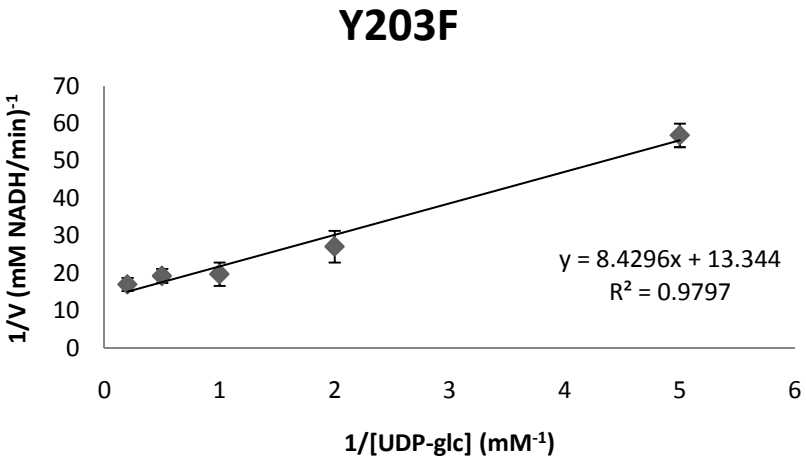
Y203F
1/V (mM NADH/min)-1
70
60
50
40
30
20
10
0
0
1
2
3
4
5
6
1/[UDP-glc] (mM-1)
y = 8.4296x + 13.344
R² = 0.9797

G

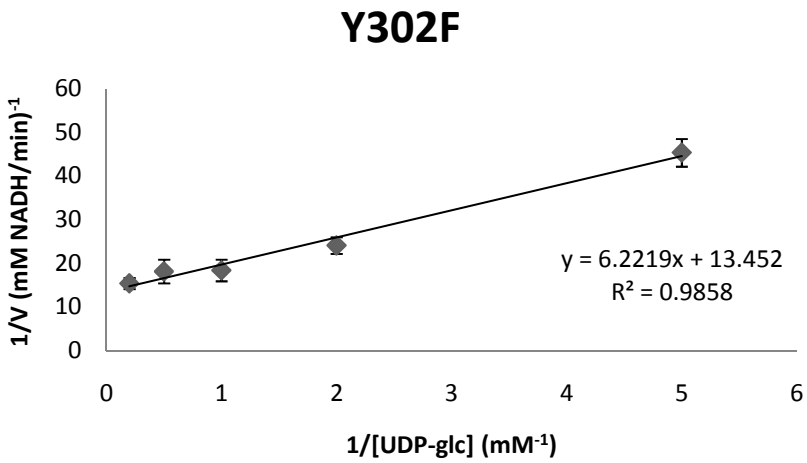

Fig. 7. Lineweaver–Burk plot of the wild type Ugd and its derivatives at five different concentration of UDP-glc. The double reciprocal plot of the wild type Ugd and the derived mutants at five UDP-glc concentrations are shown. The intercept on the ordinate is equal to $1/V_{max}$, and the intercept on the abscissa is equal to $-1/K_m$. The data represent the mean ± SD of triplicate difference experiment. (A) Ugd WT, (B) Y53F, (C) Y71F, (D) Y76F, (E) Y85F, (F) Y203F, (G) Y302F

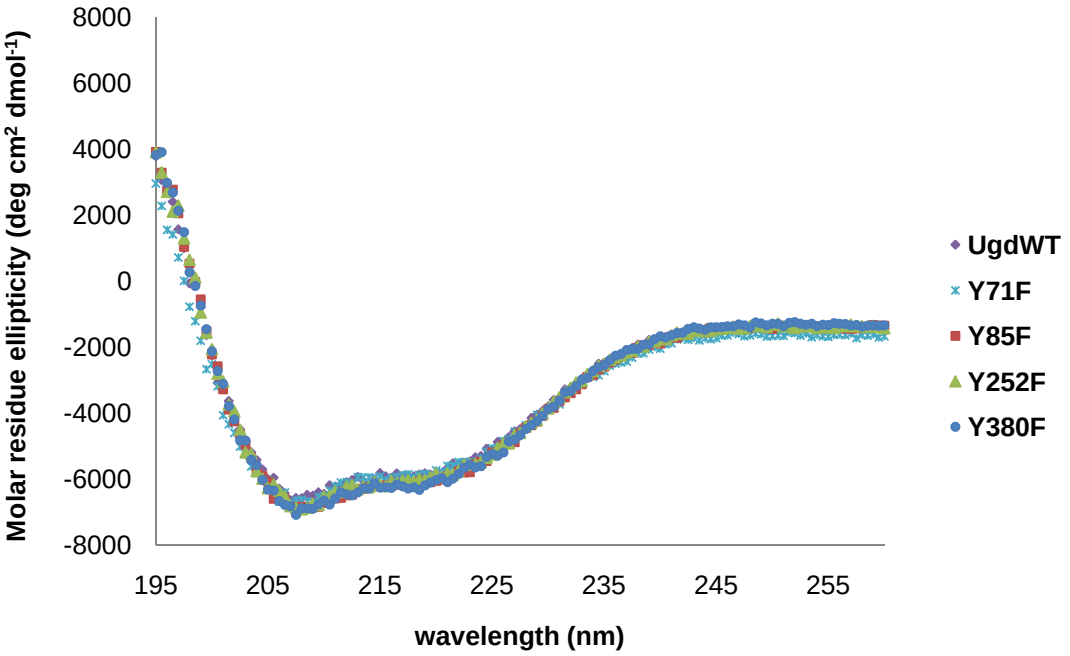

Fig. 8. Circular dichroism spectra of the wild-type and mutant Ugd. The CD spectra signals were collected from 195 nm to 260 nm in 10 mM Tris–HCl at 25 °C and averaged over three scans.

A

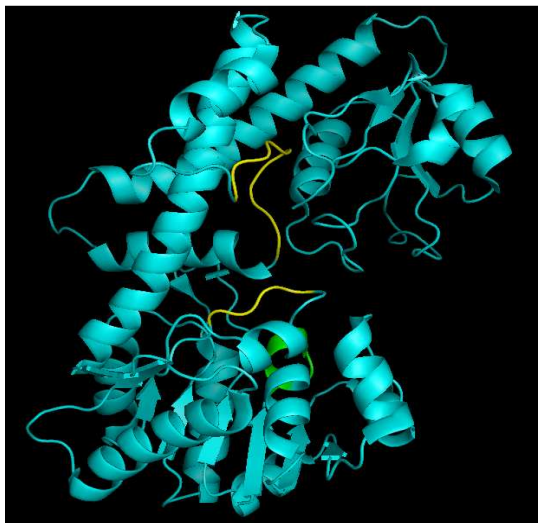

B

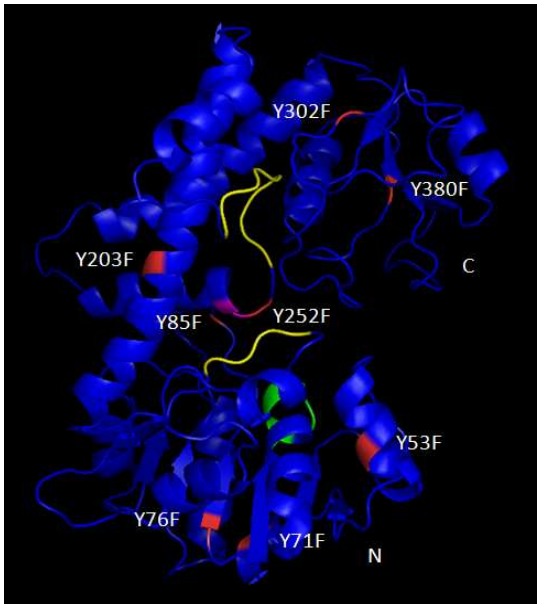

Fig. 9. Three-dimensional structure of the Ugd protein. (A) Structure of *S. pyogenes* Ugd. (B)The predicted structure for *K. pneumoniae* Ugd. Eight tyrosine residues (including Y53, Y71, Y76, Y85, Y203, Y252, Y302 and Y380) are shown in red. The Ugd catalytic site residue, Cys253, is shown in magenta. N means the N terminus and C means the C terminus of the polypeptide. UDP-glc binding site is colored yellow and NAD^+ binding site is colored green (Campbell, 2000).

A

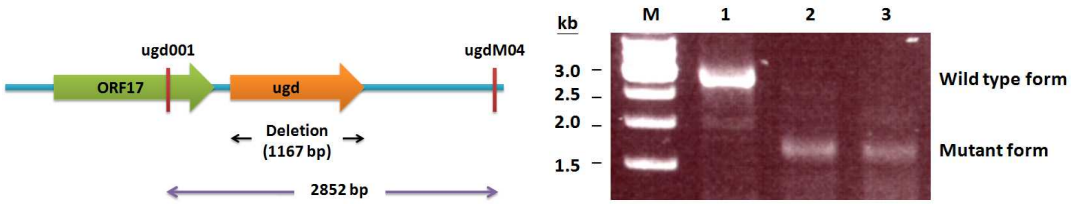
ugd001
ugdM04
ORF17
ugd
Deletion
(1167 bp)
2852 bp
kb
M
1
2
3
3.0
2.5
2.0
1.5
Wild type form
Mutant form

B

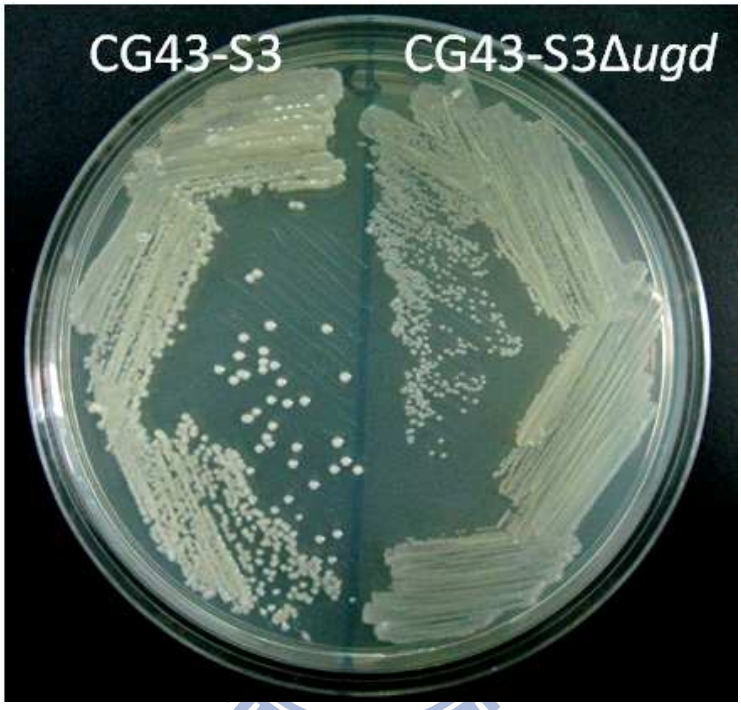
CG43-S3
CG43-S3Δugd

C

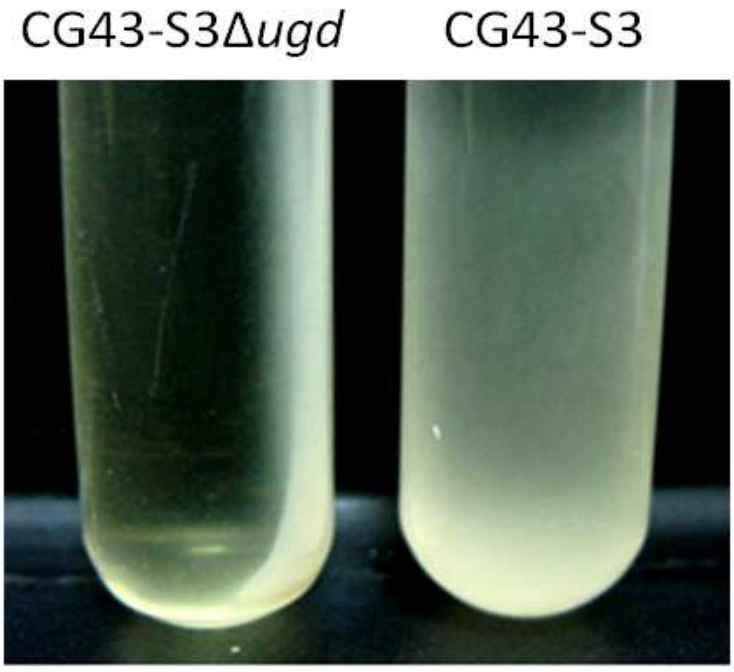
CG43-S3Δugd
CG43-S3

Fig. 10. Construction of the *ugd*-deletion mutant (A) and phenotype analysis of the mutant (B and C). (A) Identification of *ugd*-deletion mutant by PCR. Lanes: 1, *K. pneumoniae* CG43-S3; lane 2: pHY034; lane 3, *K. pneumoniae* CG43-S3 Δugd (B) Colony morphology of wild type strain CG43-S3 and CG43-S3Δ*ugd*. Photographs were taken after wild type strain CG43-S3 and CG43-S3Δ*ugd* grown on LB agar plate for 16 h at 37°C. (C) Overnight culture of wild type strain CG43-S3 (right) and CG43-S3Δ*ugd* (left) were subjected to sedimentation rate test with 4000 rpm (1,500 × *g*) centrifugation for 3 min.

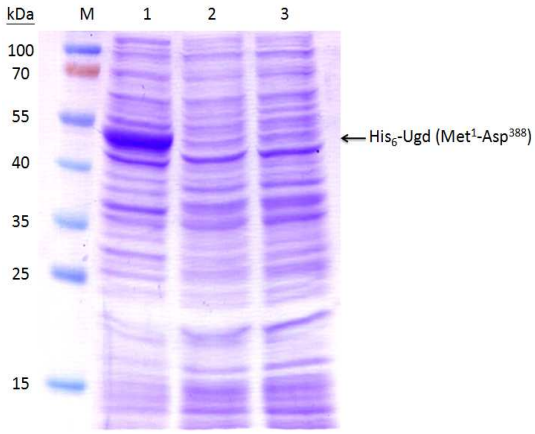

Fig. 11. Expression of pET-30b-Ugd in *E. coli* and *K. pneumoniae*. Total proteins isolated from the *E. coli* NovaBlue (DE3) and *K. pneumoniae* CG43 carrying each of the recombinant clones of pET-30b-Ugd were subjected to SDS-PAGE and visualized by staining with Coomassie Brilliant Blue. Lane M: molecular weights standards. The molecular mass labeled in kDa is shown on the left. Lanes 1 pET-30b-Ugd in *E. coli* NovaBlue (DE3); 2, pET-30b in *K. pneumoniae* CG43; and 3, pET-30b-Ugd in *K. pneumoniae* CG43.

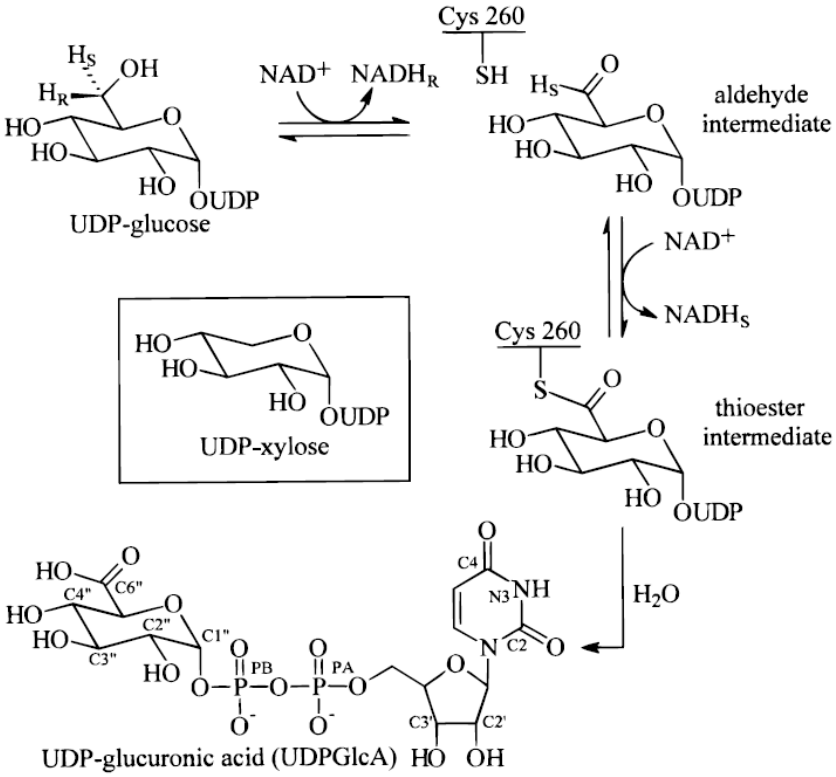

Appendix 1. Schematic diagram presentation of the Ugd catalytic reaction. (Campbell *et al*., 2000)

A

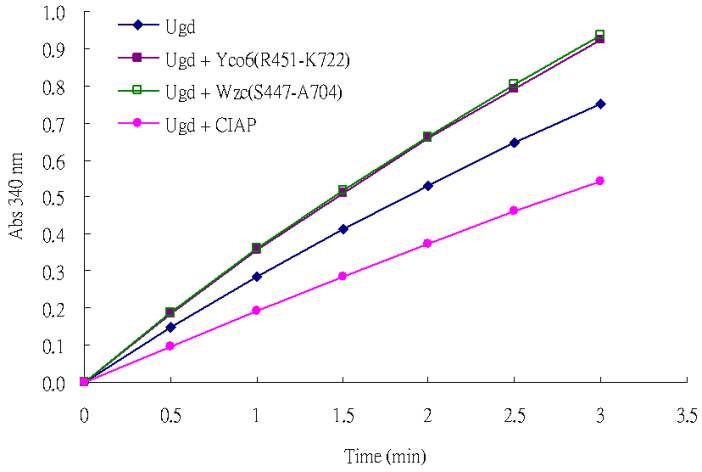

B

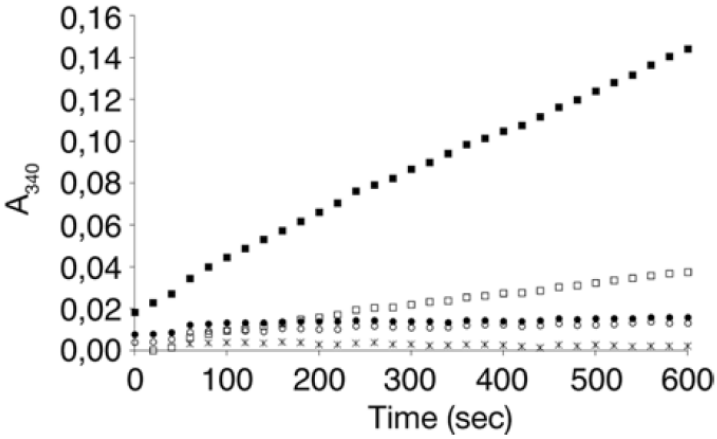

Appendix 2. Activation of the UDP-glucose dehydrogenase activity of Ugd by phosphorylation. (A) His_6-*Kp*Ugd (◆), His_6-*Kp*Ugd previously phosphorylated by His_6-Yco6(Arg^{451}-Lys^{722}) (■), His_6-*Kp*Ugd previously phosphorylated by His_6-Wzc(Ser^{447}-Ala^{704}) (□), His_6-*Kp*Ugd previously treated with calf intestine alkaline phosphatase (CIAP) (●) (Zhi-Kai Li, 2005). (B) *E. coli* Ugd (□), Ugd previously phosphorylated by Wzc_{cyto} (■), UgdY71F (○) and UgdY71F previously incubated with Wzc_{cyto} (●). As a control, a reaction mixture without Ugd was used (*) (Lacour *et al.*, 2008).

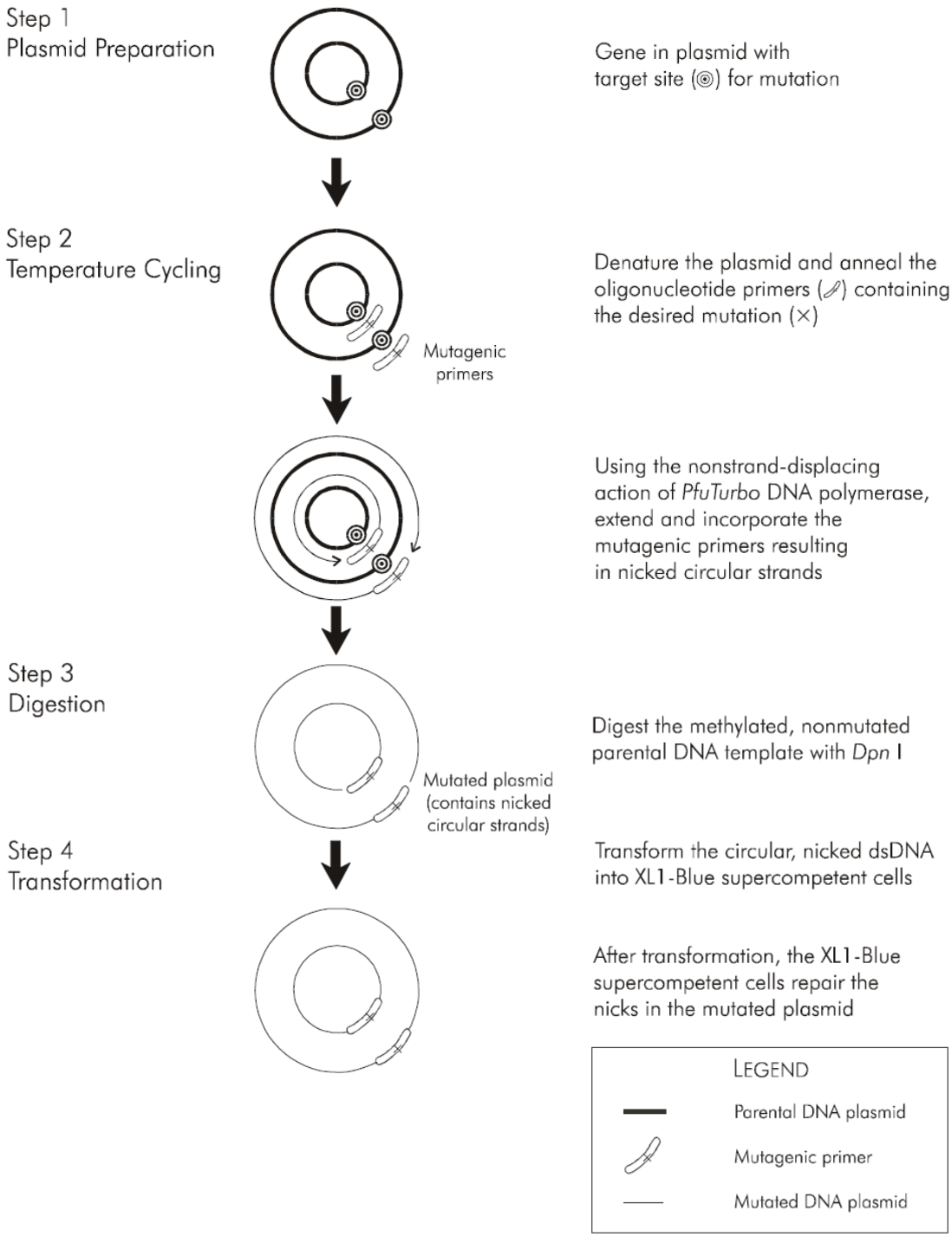

Appendix 3. Overview of the QuikChange site-directed mutagenesis method assay (QuikChange® site-directed mutagenesis instruction manual, Stratagene).

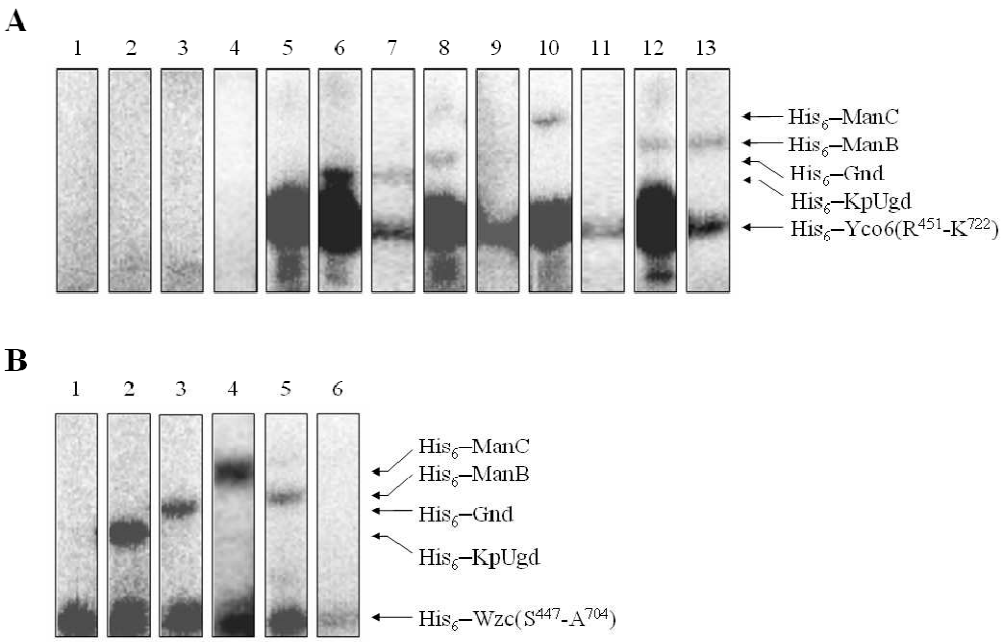

Appendix 4. *In vitro* phosphorylation. Autoradiography of *in vitro* phosphorylation and dephosphorylatoin assays separated on SDS-PAGE. The lanes contained reaction mixtures and [γ-^{32}P] ATP with the following proteins: **(A)** His_6-*Kp*Ugd (lane 1), His_6-Gnd (lane 2), His_6-ManC (lane 3), His_6-ManB (lane 4), His_6-Yco6(Arg^{451}-Lys^{722}) (lane 5), His_6-Yco6(Arg^{451}-Lys^{722}) and His_6-*Kp*Ugd (lane 6), His_6-Yco6(Arg^{451}-Lys^{722}), His_6-*Kp*Ugd and His_6-Yor5 (lane 7), His_6-Yco6(Arg^{451}- Lys^{722}) and His_6-Gnd (lane 8), His_6-Yco6(Arg^{451}-Lys^{722}), His_6-Gnd and His_6-Yor5 (lane 9), His_6-Yco6(Arg^{451}-Lys^{722}) and His_6-ManC (lane 10), His_6-Yco6(Arg^{451}- Lys^{722}), His_6-ManC and His_6-Yor5 (lane 11), His_6-Yco6(Arg^{451}- Lys^{722}) and His_6-ManB (lane 12), His_6-Yco6(Arg^{451}-Lys^{722}), His_6-ManB and His_6- Yor5 (lane 13). **(B)** His_6-Wzc(Ser^{447}-Ala^{704}) (lane 1), His_6-Wzc(Ser^{447}-Ala^{704}) and His_6-*Kp*Ugd (lane 2), His_6-Wzc(Ser^{447}-Ala^{704}) and His_6-Gnd (lane 3), His_6-Wzc (Ser^{447}-Ala^{704}) and His_6-ManC (lane 4), His_6-Wzc(Ser^{447}-Ala^{704}) and His_6-ManB (lane 5), His_6-Wzc (Ser^{447}-Ala^{704}) and His_6-Yor5 (lane 6) (Zhi-Kai Li, 2005).

A

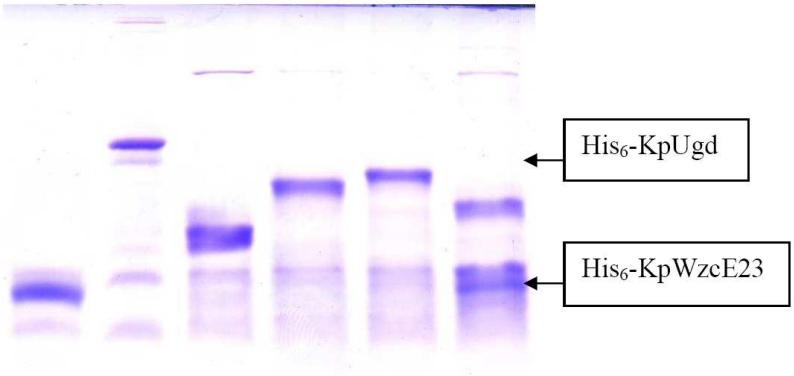

B

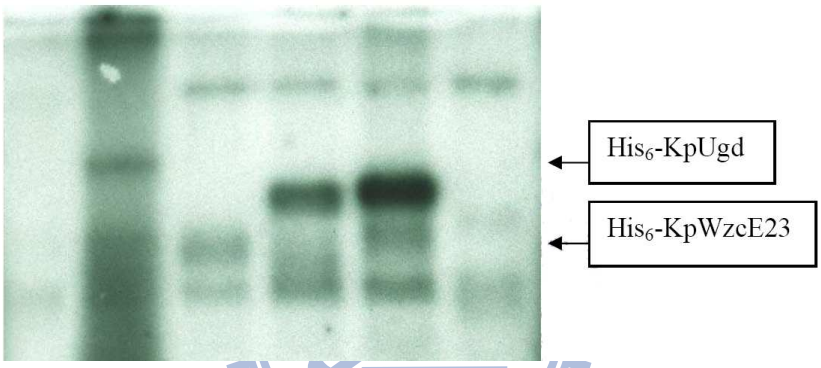

Appendix 5. *In vitro* phosphorylation of His$_6$-*Kp*Ugd and GST-*Kp*Ugd fragments. Autoradiography of *in vitro* phosphorylation assays separated on SDS-PAGE. The lanes contained reaction mixtures and [γ-^{32}P] ATP with the following proteins: lane1, GST and His$_6$-*Kp*WzcE23; 2, His$_6$-*Kp*Ugd and His$_6$-*Kp*WzcE23; 3, GST-*Kp*Ugd1 (Met^{1} to Lys^{67}) and His$_6$-*Kp*WzcE23; 4, GST-*Kp*Ugd2 (His^{68} to Ala^{167}) and His$_6$-*Kp*WzcE23; 5, GST-*Kp*Ugd3 (Glu^{168} to Gly^{300}) and His$_6$-*Kp*WzcE23; 6, GST-*Kp*Ugd4 (Val^{301} to Asp^{388}) and His$_6$-*Kp*WzcE23 (Han-Sheng Chien, 2008).